



ELSEVIER

Available online at www.sciencedirect.com
jmr&t
 Journal of Materials Research and Technology
journal homepage: www.elsevier.com/locate/jmrt**Original Article**

Effect of ultrasonic field on microstructure evolution in friction stir welding of dissimilar Al/Mg alloys

**Junjie Zhao, ChuanSong Wu^{*}, Lei Shi**

MOE Key Lab for Liquid-Solid Structure Evolution and Materials Processing, Institute of Materials Joining, Shandong University, Jinan, 250061, China

ARTICLE INFO**Article history:**

Received 23 October 2021

Accepted 28 December 2021

Available online 4 January 2022

Keywords:

Grain microstructure evolution

Aluminum alloy

Magnesium alloy

Friction stir welding

Ultrasonic vibration

ABSTRACT

Understanding of the microstructure evolution and the influence of ultrasonic vibration on friction stir welding (FSW) of dissimilar Al/Mg alloys is of great significance in optimizing the process parameters and improving the joint quality. In this study, the microstructure evolutions in the weld nugget zone (WNZ) of dissimilar Al/Mg joints during FSW and ultrasonic vibration enhanced FSW (UVeFSW) were characterized and compared. It was found that ultrasonic vibration (UV) has great effect on the grains structure of the WNZ in the Mg alloy side. Specially, the exerted UV changed the main dynamic recrystallization (DRX) mechanism of grains in the Mg alloy side from continuous DRX (CDRX) to discontinuous DRX (DDRX) under lower or higher welding speeds but constant tool rotation speed. Along the thickness direction, the average grain sizes near the bonding interface in the WNZ increased first and then decreased, and the maximum grain size was located at the mid-depth of the weld. Low strain shear texture appeared more in the WNZ of the Al alloy side during FSW, while in UVeFSW more locations in the WNZ were with high strain shear textures. The application of UV field improved the DRX degree in the whole weld through promoting the entanglement, aggregation and rearrangement of dislocations.

© 2021 The Author(s). Published by Elsevier B.V. This is an open access article under the CC BY-NC-ND license (<http://creativecommons.org/licenses/by-nc-nd/4.0/>).

1. Introduction

Lightweight structure of transportation vehicles is an effective way to achieve energy conservation and emission reduction. To this end, lightweight materials like Al alloys and Mg alloys have been used more and more in automobile industry. This has inevitably led to challenges in joining Al alloys and Mg alloys, and dissimilar welding is able to employ the

advantages of both materials simultaneously [1]. Friction stir welding (FSW), as a solid-state process, is especially suitable for joining dissimilar Al/Mg alloys. It can avoid defects caused by melting/solidification in fusion welding and produce very low residual stress and distortion [2–4].

During the FSW process with intense plastic deformation and frictional heating, dynamic recrystallization (DRX) can occur in three types: continuous dynamic recrystallization

* Corresponding author.

E-mail address: wucs@sdu.edu.cn (C. Wu).<https://doi.org/10.1016/j.jmrt.2021.12.133>2238-7854/© 2021 The Author(s). Published by Elsevier B.V. This is an open access article under the CC BY-NC-ND license (<http://creativecommons.org/licenses/by-nc-nd/4.0/>).

(CDRX), discontinuous dynamic recrystallization (DDRX) and geometric dynamic recrystallization (GDRX) [5–7]. DRX during FSW has an important effect on the grain microstructure refinement in the weld nugget zone (WNZ). For FSW of the same metal (Al alloy or Mg alloy), the resultant grain structure in the weld is usually the main factor affecting the joint strength. For dissimilar FSW of Al/Mg alloys, the joint strength primarily depends on metallurgical bonding by formation of intermetallic compounds (IMCs) and mechanical interlocking due to the tortuous bonding interface [1,2,8,9]. The amount and thickness of brittle IMCs have to be controlled within appropriate ranges [10]. On the other hand, the microstructures in dissimilar welds are still critical to determine the joint quality, and the abnormal grain structure will also severely affect the properties of the joints. At the same time, the corrosion resistance of the joints is dependent on the grain microstructure in WNZ [11,12]. Therefore, the evolution of grain structures in dissimilar welds should be deeply investigated. However, previous studies only focused on the microstructure evolution of the same metal FSW welds [5–8]. For dissimilar FSW of Al/Mg alloys, the different thermodynamic properties of two materials and the IMCs formation will result in different characteristics of grain structures.

Recently, in order to suppress the generation of IMCs and alleviate the influence of some inherent problems in FSW on joint strength [13], some modified FSW process have been proposed, such as under liquid nitrogen or underwater FSW [14,15]; water cooling assisted FSW [16]; heat assisted FSW [17]; and hybrid laser friction stir welding [18]. Nonetheless, such modifications increased the operation difficulty and cost, which hinders their application in practice. Since ultrasonic vibration (UV), as a kind of mechanical energy, can lower the yield strength of materials during plastic deformation, UV has been applied to assist FSW of Al/Mg alloys [19–21]. As for the exertion mode of UV, Benfer et al. [19] applied UV on one base material via a roller, while Ji et al. [20] and Liu et al. [21] placed an ultrasonic generator toward the bottom of Mg plates. The authors' group developed a different system, which applies UV directly on the top surface of base materials and in front of the tool, namely the ultrasonic vibration enhanced friction stir welding (UVeFSW) [10,22]. Our previous studies have shown that the ultrasonic field cannot only promote the mixing of Al and Mg materials, but also inhibit the growth of IMCs, so as to significantly improve the joint strength in Al/Mg dissimilar FSW [10,23–25]. However, the underlying mechanism of UVeFSW in dissimilar Al/Mg alloys and its influence on the microstructure evolution have not been elucidated.

In this work, the FSW and UVeFSW butt welding of dissimilar Al/Mg alloys were carried out, and the grain structures

in different regions of the welds under different welding conditions were characterized. The grain size, misorientation angle distributions and textures on both sides of bonding interface were compared. The DRX mechanisms at different locations in WNZ were analyzed, and the influence of UV on the grain structure evolution in dissimilar FSW of Al/Mg alloys were discussed.

2. Experimental

6061-T6 Al alloy and AZ31B–H24 Mg alloy plates with a thickness of 3 mm were butt welded. Their chemical composition and mechanical properties are listed in Table 1. Fig. 1 shows the experimental set-up. The ultrasonic vibration was directly acted on the workpieces in front of the tool via the sonotrode with an angle of 40° relative to the workpiece surface and a distance of 20 mm away from the tool axis. In this experiment, the UV frequency was 20 kHz, and the output power was about 220 W. Conventional FSW and UVeFSW experiments were made to compare the difference of microstructure evolution in dissimilar Al/Mg alloys WNZs.

According to the experimental optimization results, the test conditions were as follows: the tool rotating speed was 800 rpm, the welding speeds ranged from 30 to 80 mm/min, the tilt angle of the tool was 2.5°, and the plunge depth of the shoulder was 0.15 mm. Mg alloy plates were placed on the advancing side (AS) while Al plates were on the retreating side (RS), and the pin was offset to the Mg alloy side by 0.3 mm. The tool used, made of H13 tool steel, consisted of a concave shoulder with a diameter 12 mm and a cone-shaped pin with right-hand thread. The tip and root diameters of pin were 3.2 and 4.2 mm, respectively, and the length was 2.75 mm. For description convenience, C is used to represent the conventional FSW tests, while U is used to represent the UVeFSW tests, that is, C-800-30 means the conventional FSW test with process parameters 800 rpm-30 mm/min, while U-800-50 means the UVeFSW test with process parameters 800 rpm-50 mm/min.

After welding, the metallographic samples were cut by electric spark wire cutting machine. Then, samples were grounded and polished with different sets of emery papers up to 1000 grit and followed by 0.5 μm diamond slurry. For electron backscattered diffraction (EBSD) characterization, the ion beam slope cutter (Leica EM TIC 3 ×) was used to remove the surface stress of the samples. The field emission scanning electron microscope (FE-SEM) (Zeiss Gemini 500) was used to collect the grain microstructure information in the weld. In the process of EBSD characterization, the scanning step size

Table 1 – Nominal composition and mechanical properties of base material.

Alloy	Nominal chemical composition (wt. %)								Mechanical properties		
	Si	Fe	Cu	Mn	Mg	Cr	Ti	Zn	Al	UTS (MPa)	EL (%)
6061-T6	0.51	0.20	0.30	0.009	1.09	0.13	—	0.05	Bal.	294	10
AZ31B–H24	0.016	0.001	0.003	0.44	Bal.	—	—	1.10	3.05	260	12

(Note: the suppliers of 6061-T6 and AZ31B–H24 were Jinan Zhixin Aluminum Industry Co., Ltd (Jinan, China) and Luoyang Shengte Metal Products Co., Ltd. (Luoyang, China), respectively.).

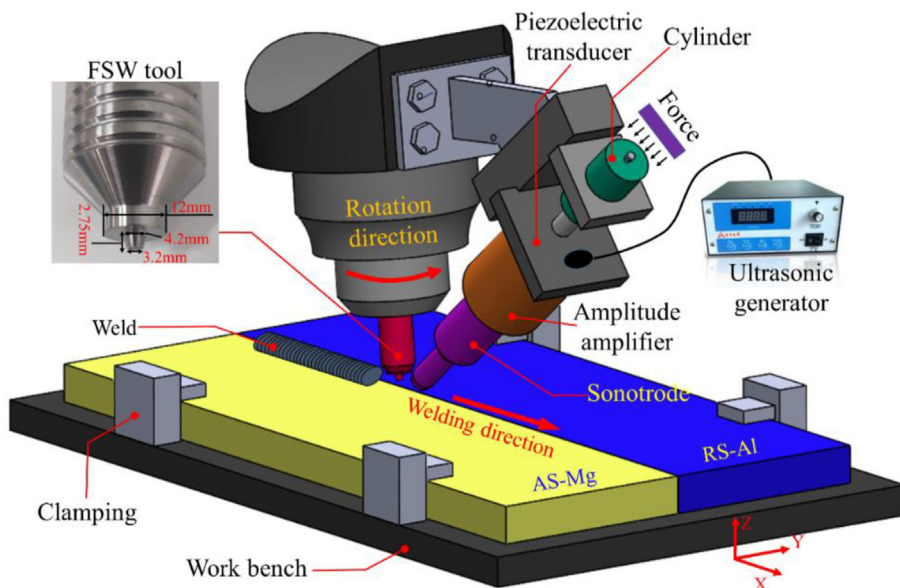


Fig. 1 – Schematic of the FSW and UVeFSW of dissimilar Al/Mg alloys.

was 0.1 μm for the regions in WNZ and 0.3 μm for the thermal mechanical affected zone (TMAZ).

For macrostructure observation, the Al alloy side was etched firstly by Keller reagent (1 ml HF + 1.5 ml HCl + 2.5 ml HNO_3 + 95 ml H_2O) for 5 s. Then, the Mg alloy side were etched by picric acid solution (4.2 g picric acid + 70 ml ethanol + 10 ml acetic acid + 10 ml H_2O) for 10 s. The macrographs of the welds were taken by Zeiss Daheng Invasion USB camera microscope.

3. Results and discussion

3.1. Microstructure of base materials

Fig. 2 shows the microstructure of base materials (6061-T6 Al alloy and AZ31B-H24 Mg alloy). The grains in Al alloy are long strips, as shown in Fig. 2a, and the average grain size is ~32.8 μm . The grain boundary information is shown in Fig. 2b, where the green boundaries represent low angle grain boundaries (LAGBs) and the black boundaries represents high angle grain boundaries (HAGBs). Most of the grain boundaries in Al base material are HAGBs, and the proportion of LAGBs is only 3.9%. Moreover, it can be seen from the misorientation angle distributions (Fig. 2c) that the grain orientation is close to random distribution. This illustrates that the grains in Al base material did not have preferred orientation during growth, which can also be found from the pole figures of Al base material (Fig. 3a), with no obvious texture formed.

As shown in Fig. 2d, the Mg alloy base material contains both coarse grains (up to about 65 μm) and very fine grains (about 1 μm), which is the typical structure of hot-rolled Mg alloy [26], and the average grain size is ~5 μm . Moreover, different from the Al base material, Mg base material contains a large number of LAGBs (Fig. 2e), and its proportion is 47.6%. At the same time, there are some twin grains in Mg base material, and a peak value at about 86° in misorientation angle distributions histogram (Fig. 2f), indicating that these twin

grains are {101-2}<1-011> tensile twins. In addition, according to the pole figures (Fig. 3b), it can be determined that there is no obvious special texture in Mg base material, only the deflected {0001} basal texture, and the maximum texture intensity is 11.36 multiple of random density (MRD).

3.2. Bonding interface morphology

Fig. 4 shows the macrograph of the welds at transverse cross-section in FSW and UVeFSW. Different from the case of same material FSW, there is an obvious bonding interface in the WNZ of dissimilar Al/Mg alloys. The tortuous interface indicates that the Al and Mg strips interpenetrated with each other in WNZ, and formed mechanical interlocking structures. It can be found that when UV was applied, the length of bonding interface increased, that is, the degree of mutual mixing of materials increased. This is related to the acoustic softening effect of UV, which reduces the material flow stress and promotes the material flow in the WNZ [10].

At the same time, the metallurgical bonding was achieved by formation of the IMCs along the bonding interface. Therefore, the existence of Al/Mg bonding interface has an important impact on the joint strength. In this study, the observation of grain structure in the WNZ was mainly carried out along this interface. As schematically illustrated in Fig. 4g, the small red and yellow squares near the bonding interface indicate the EBSD observation positions on the Al side and the Mg side, respectively.

3.3. Grain structure at mid-depth locations under different welding speeds

3.3.1. Grain microstructure at A3 in the WNZ of the Al side
Firstly, the grains at the WNZ in the Al side, i.e., location A3 in Fig. 4g, was characterized by EBSD. Fig. 5 shows the obtained grain microstructure morphology at A3 in FSW and UVeFSW under three levels of welding speed. In Fig. 5, the black grain

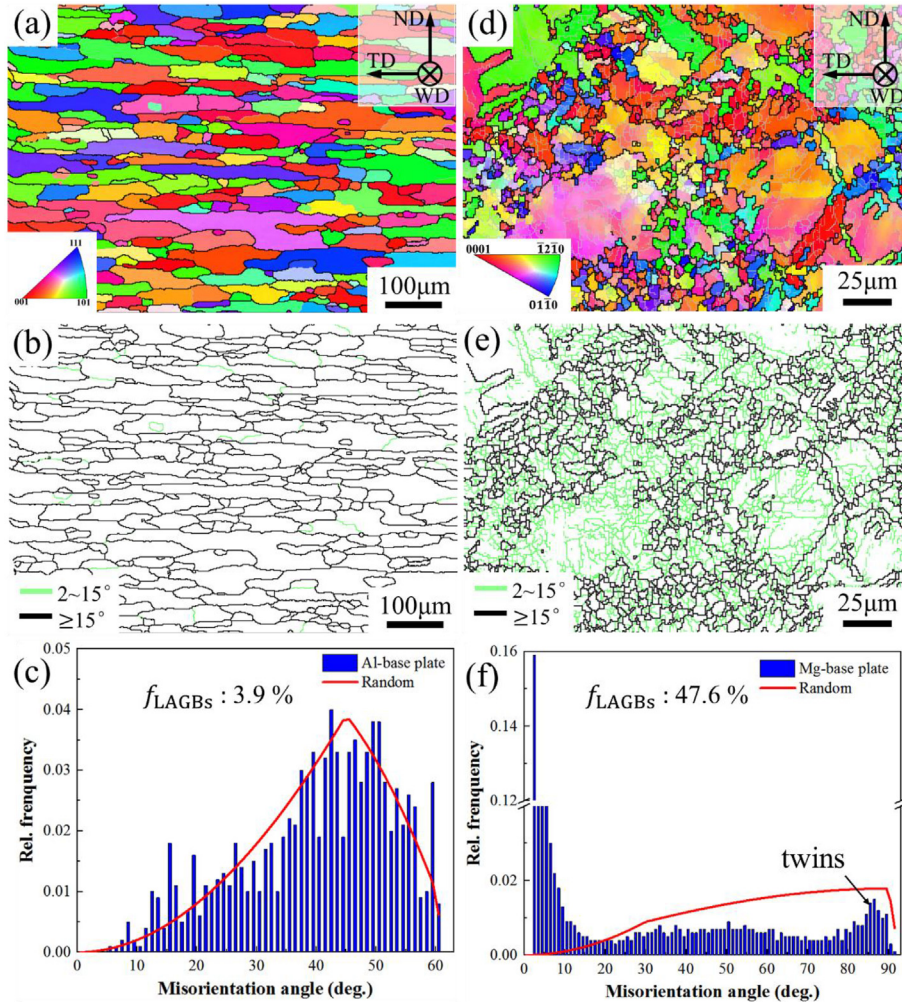


Fig. 2 – IPF maps, GB maps and misorientation angle distributions of base materials (a, b, c): Al alloy; (d, e, f): Mg alloy.

boundaries were the HAGBs, the silver gray grain boundaries were the LAGBs, and the division value between them was 15°. Regardless of FSW or UVeFSW, fine grains were formed in the WNZ on the Al side. When the welding speed was 30 mm/min, the grains had an obvious inclined downward deformation orientation, as shown by the black dotted line in Fig. 5a and b. Since the pin used in this study was cone-shaped with right-hand thread, the counterclockwise rotation of the pin during welding was conducive to promoting the downward flow of material [27], so that the grains had an inclined downward deformation orientation. When UV was applied in UVeFSW, such inclination angle was decreased, which may be due to the fact that UV field can effectively enhance the material flow in horizontal direction [21]. However, there was no inclined downward deformation orientation under other two welding speeds (50 and 80 mm/min), which may be because the material cannot flow downward effectively at the higher welding speed. The more specific reason requires a further detailed exploration of the material flow in Al/Mg dissimilar FSW.

The fine grains in the WNZ of the Al side were obviously produced by DRX. It can be found that the boundaries of most grains were composed of some LAGBs and some HAGBs, such as the grains in the white circles in Fig. 5, which is a typical

feature of CDRX [28]. In addition, it can also be observed that some elongated grains were decomposed into several subgrains, which formed a LAGB with little difference in grain orientation, as shown by the black arrows in Fig. 5. This illustrates that GDRX also played a certain role [29], but CDRX should be the dominant mechanism of grain DRX.

According to statistics of grain size in Fig. 5, for FSW with welding speed of 30, 50 and 80 mm/min, the average grain size in Al side WNZ was 0.92 ± 0.21 ; 1.18 ± 0.24 ; and $0.86 \pm 0.24 \mu\text{m}$, respectively. In UVeFSW, the corresponding average grain size was 0.79 ± 0.18 ; 0.98 ± 0.22 and $0.96 \pm 0.26 \mu\text{m}$, respectively. It can be found that after application of UV field, the grain size was refined at the welding speed of 30 and 50 mm/min, but it coarsened a little bit at the welding speed of 80 mm/min. However, the change of grains size with and without application of UV is small. This is because the thermo-mechanical action in FSW already refines the grains in WNZ to a considerable degree. The exerted UV, which just plays an auxiliary role, can only cause the change of grains size to a certain extent. It should be noted that the grain size in the WNZ of the Al side was very small (about 1 μm) in both cases of dissimilar FSW and UVeFSW. Usually, in FSW of the same Al alloys (6061-T6) under the same rotation speed and higher welding speed,

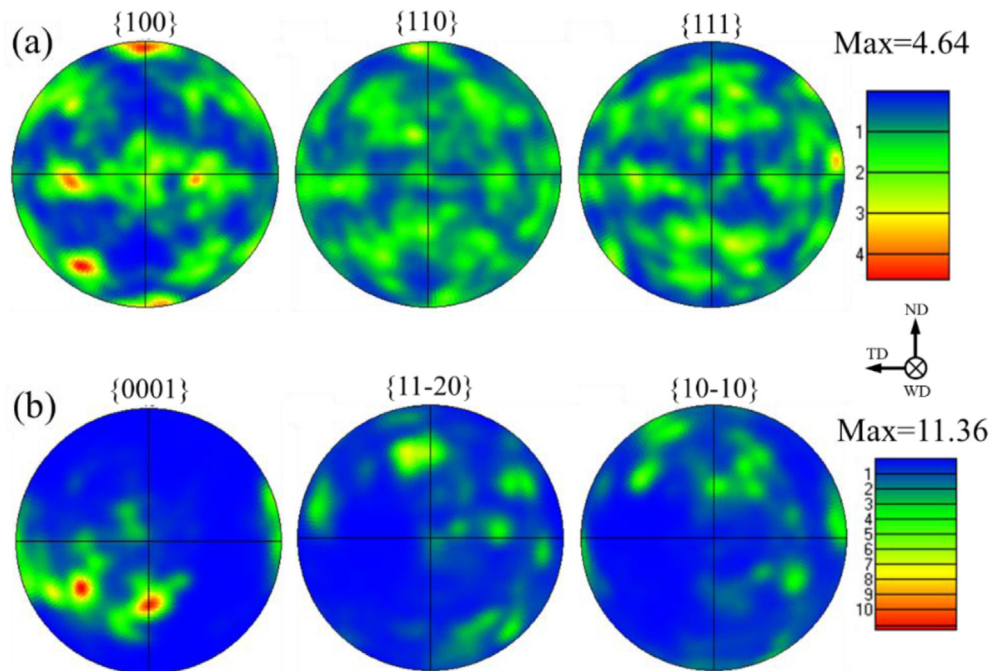


Fig. 3 – Pole figures of base materials. (a) Al alloy, (b) Mg alloy.

the minimum average grain size in the WNZ was greater than $2 \mu\text{m}$ [30]. This is because the temperature in WNZ during FSW of Al alloy is usually higher than that during dissimilar FSW of Al/Mg alloys [2].

In addition, the average grain size increased first and then decreased with the increase of welding speed in both FSW and UVeFSW, although the grain size difference between 50 and

80 mm/min cases was very small in UVeFSW. Generally, the lower the welding speed is, the higher the welding heat input is, and the easier for grain to grow. The reason for this is that the recrystallized grain size in the WNZ is not only dependent on the temperature, but also dependent on the strain rate of material deformation. The specific relationship can be expressed by following equations [31–33].

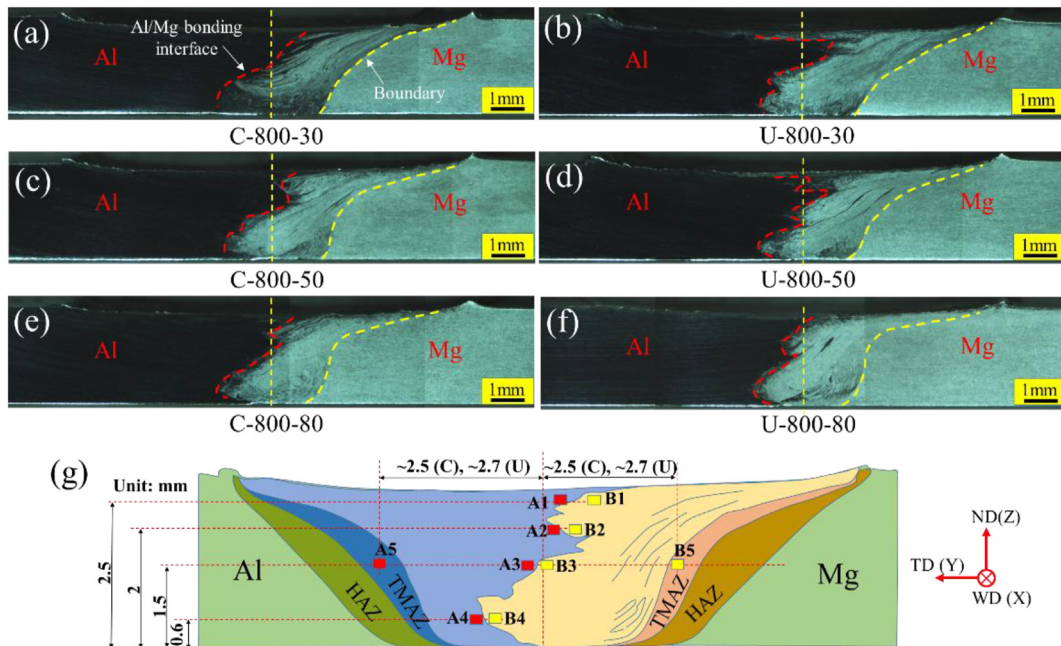


Fig. 4 – The weld morphology in FSW (a, c, e) and UVeFSW (b, d, f), and schematic of EBSD data acquisition locations near bonding interface (g).

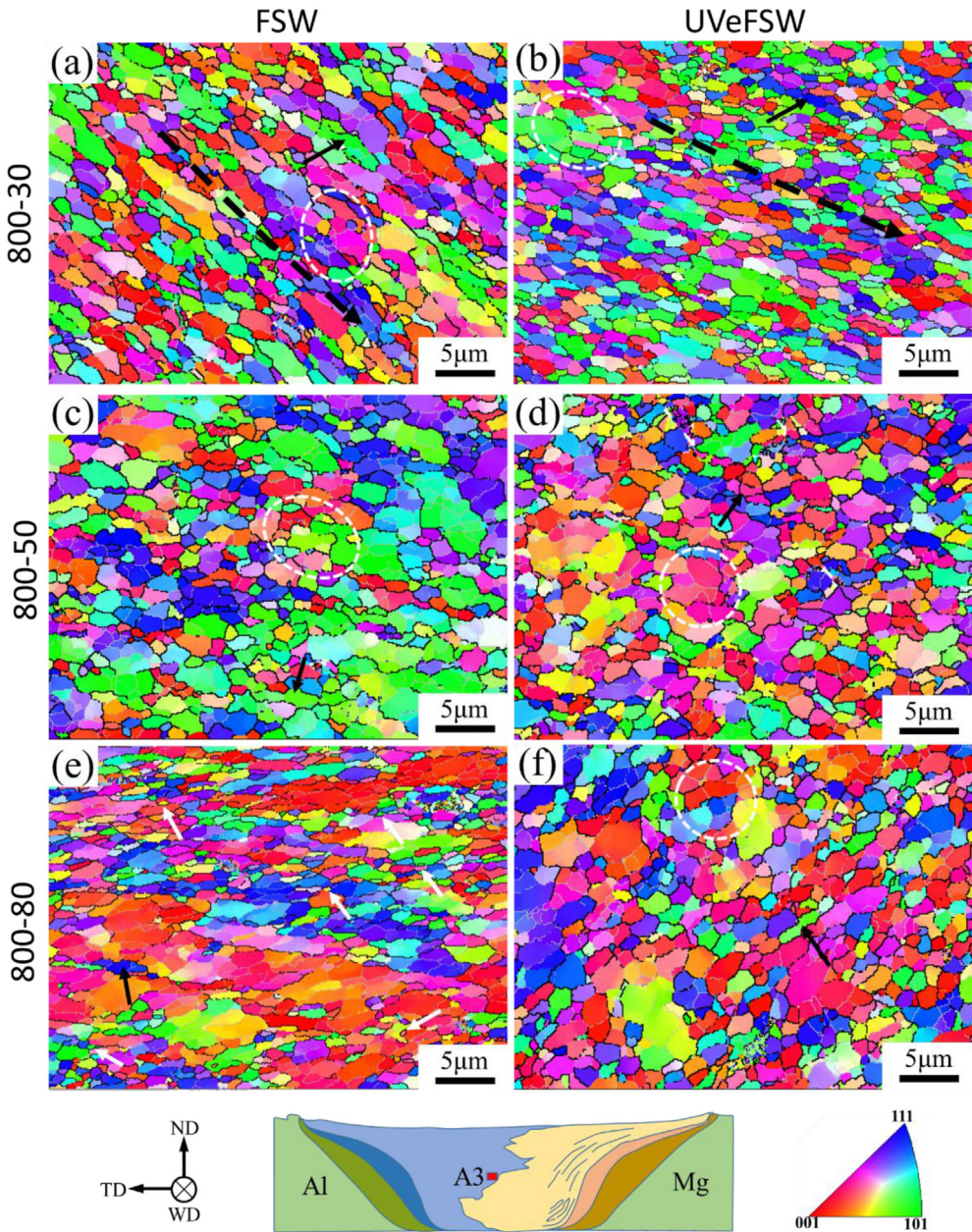


Fig. 5 – IPF maps of grain microstructures at location A3 (the WNZ in the Al side) in FSW and UVeFSW under different weld speeds.

$$\frac{d_{WNZ}}{d_{BM}} = 10^3 \cdot Z^{1/3} \quad (1)$$

$$Z = \dot{\varepsilon} \cdot \exp(Q / RT) \quad (2)$$

$$\dot{\varepsilon} = \frac{R_m \cdot 2\pi r_e}{L_e} \quad (3)$$

$$\frac{T}{T_m} = K \cdot \left[\frac{\omega^2}{v \cdot 10^4} \right]^\alpha \quad (4)$$

where d_{WNZ} is the grain size in WNZ, d_{BM} is the grain size in base materials, Z is the Zener-Holloman parameter, $\dot{\varepsilon}$ is the strain rate, Q is the lattice diffusion activation energy, R is the

molar gas constant, T is the temperature in WNZ, R_m is the average material flow rate (about half the rotation speed), r_e is the effective radius of dynamic recrystallization region, L_e is the effective depth of dynamic recrystallization region, T_m is the melting point of base materials, ω is the rotation speed, v is the welding speed, K and α are constants.

Based on Eqs. (1)–(4), the higher the temperature, the larger the grain size in the WNZ, while the larger the strain rate, the smaller the grain size. Therefore, when the welding speed increased, on one hand, the decreasing of temperature reduced the grain size, but on the other hand, the decrease of strain rate increased the grain size. Under the complex action of these two effects, the grain size did not change monotonously with the increase of welding speed. With applied UV

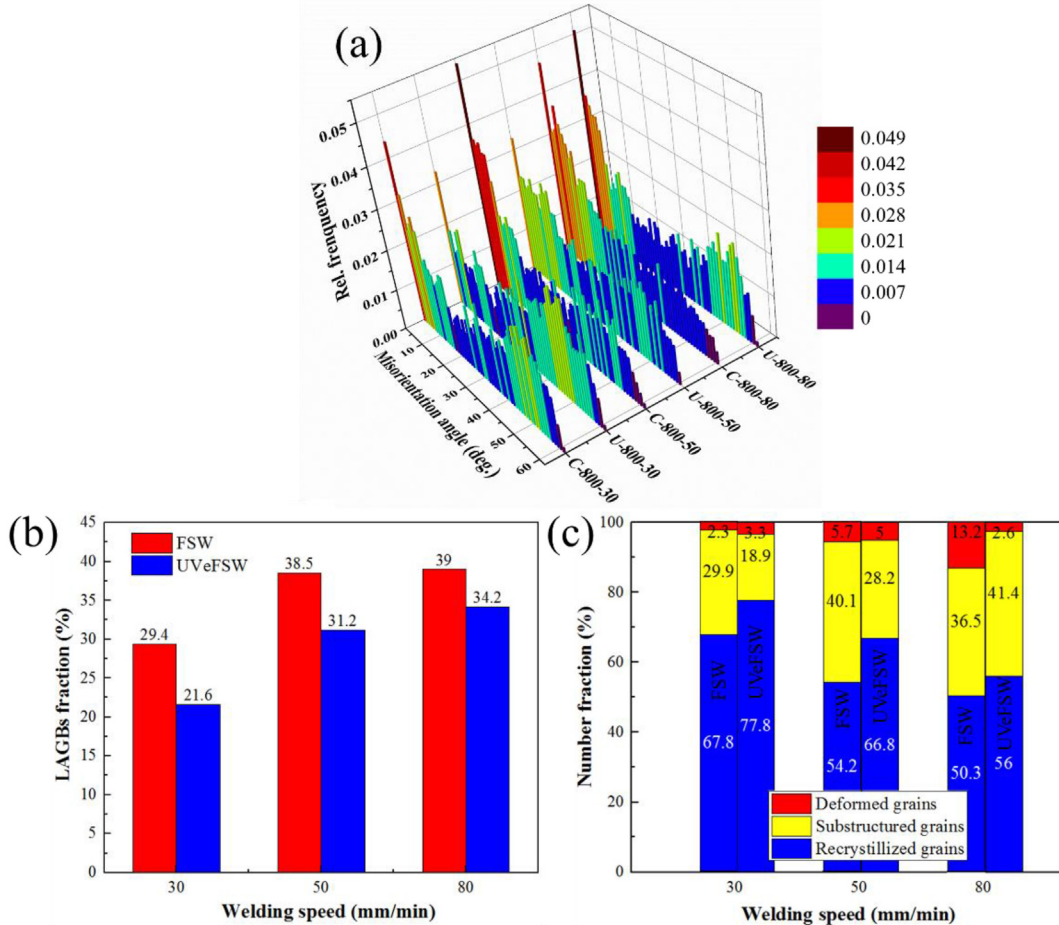


Fig. 6 – Grain microstructure information at location A3 (the WNZ in the Al side) in FSW and UVeFSW. (a) Misorientation angle distribution, (b) LAGBs fraction, (c) Comparison of recrystallization degree.

field, the acoustic softening effect can significantly reduce the deformation stress of the material, so as to promote the material deformation [34,35] and increase the strain rate [10,22,23]. Moreover, the UV field has little effect on the welding temperature [10]. Thus, theoretically, the grain size will be reduced after applying UV, which is also validated by above-mentioned test results. As for the increase of average grain size at welding speed of 80 mm/min, it will be discussed in detail in Section 4.

Fig. 6 shows the misorientation angle distribution, LAGBs fraction and recrystallization degree at location A3 in the WNZ of the Al side. It can be found that after the application of UV, LAGBs fraction decreased, and the recrystallization degree of grains increased, which indicates that more LAGBs were transformed into HAGBs in UVeFSW. Hu et al. [29] also found that the UV field can promote the recrystallization behavior of grains in FSW of same 2219 Al alloy, which is consistent with the results of dissimilar UVeFSW in this study. In contrast, in C-800-80, although the recrystallization degree of the grains was low, there were a large amount of extremely fine grains (as shown by the white arrows in Fig. 5e), which reduced the average grain size. When the welding speed was 30 and 50 mm/min, the grain morphology well conformed to the law that the LAGBs fraction decreases,

the recrystallization degree increases, and the grain size is refined. In addition, with the increase of welding speed, the recrystallization degree decreased gradually, which is mainly because the dislocation motion rate decreased with the decrease of welding heat input, which affected the dynamic recrystallization process.

3.3.2. Grain microstructure at B3 in the WNZ of the Mg side
The grain microstructure at location B3 in the WNZ of the Mg side is shown in Fig. 7. Different from the Al alloy side, no obvious deformation orientation of grains was found in the WNZ at welding speed of 30 mm/min, which may be due to the different recrystallization processes of Al alloy and Mg alloy. It was observed that most grain boundaries in the WNZ of the Mg side were also composed of some HAGBs and some LAGBs, as shown in the white circles marked in Fig. 7, indicating that CDRX had occurred. At the same time, some grain boundaries expanded outward and formed new grains at the grain boundary, as shown by the black arrows in Fig. 7, which accords with the typical characteristics of DDRX [36]. Therefore, the recrystallization mechanism in the WNZ of the Mg side includes CDRX and DDRX, which is consistent with the recrystallization mechanism in FSW of similar Mg alloys [36,37].

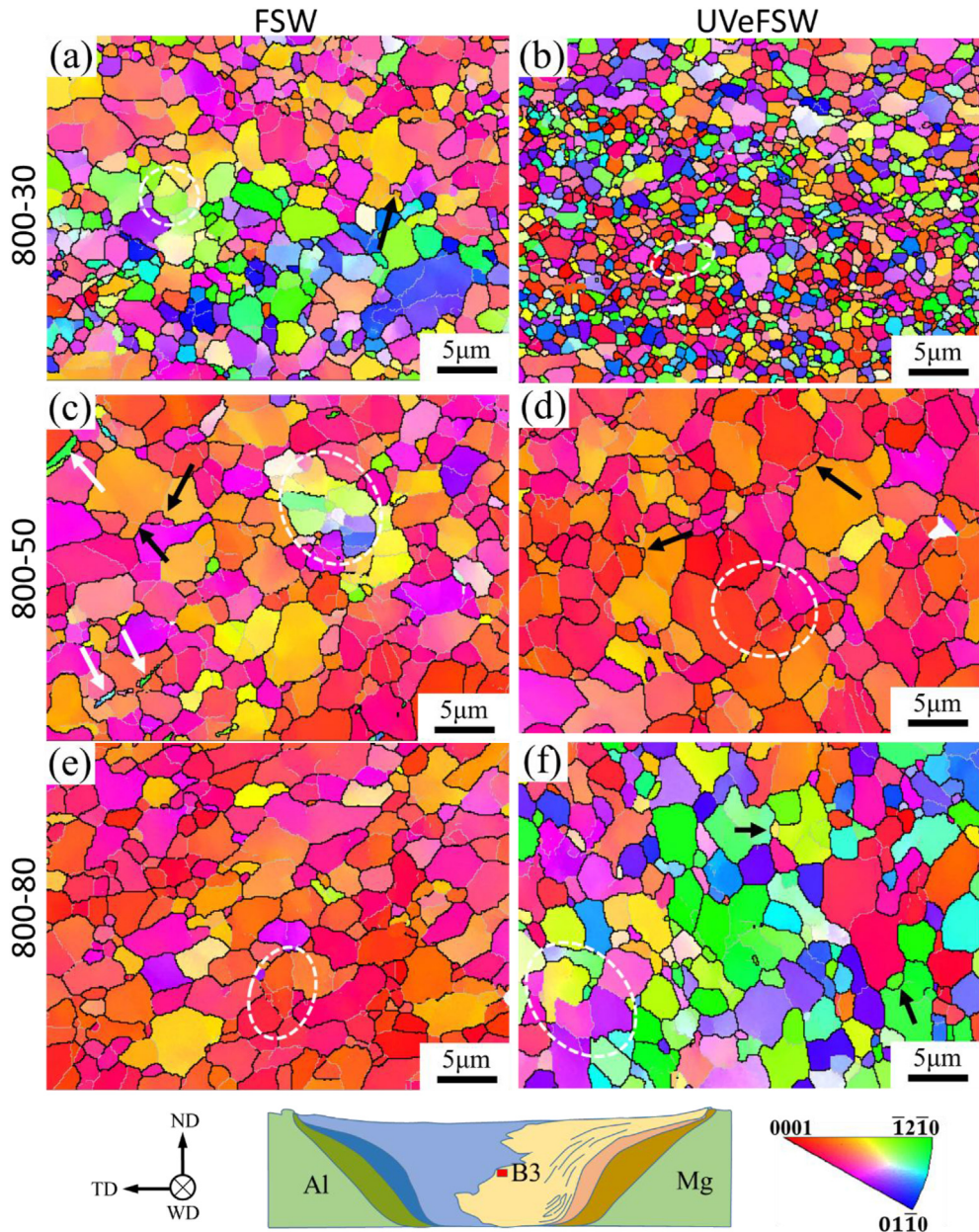


Fig. 7 – IPF maps of grain microstructures at location B3 (the WNZ in the Mg side) in FSW and UVeFSW under different weld speeds.

In FSW, when the welding speed was 50 and 80 mm/min, most grains in the WNZ of the Mg side had obvious <0001 orientation. But in UVeFSW, this phenomenon only appeared in the weld made with welding speed 50 mm/min. This may be due to the change in the degree of grains recrystallization and the material flow after the application of UV field. According to statistics of grain size in Fig. 7, the average grain size at location B3 was 1.68 ± 0.26 ; 2.57 ± 0.43 and 2.38 ± 0.36 μm in FSW under weld speed of 30, 50 and 80 mm/min, respectively. With applied UV, the average grain size at location B3 was 0.93 ± 0.19 ; 2.32 ± 0.44 and 2.02 ± 0.41 μm in UVeFSW, respectively. With the increase of welding speed, the grain size in the WNZ of the Mg side first increased and then decreased, similar to the case on the Al side. This indicates

that in the same weld, although the materials are different at two sides, the variation law of grain size affected by temperature and strain rate is the same. But the grain size at B3 (the WNZ in the Mg side) was generally larger than that at A3 (the WNZ in the Al side). This is not only related to the different stacking fault energy of Al and Mg materials, but also related to the original grain size of two base materials [28,38]. However, compared with the cases of same Mg alloy FSW or dissimilar Mg alloy FSW [36,38], the grain size in the WNZ of the Mg side is much smaller in dissimilar FSW of Al/Mg alloys. This is also due to the relatively low welding temperature in dissimilar FSW of Al/Mg alloys [2].

When the welding speed was 30 mm/min, the grain size in the WNZ of the Mg side changed greatly before and after the

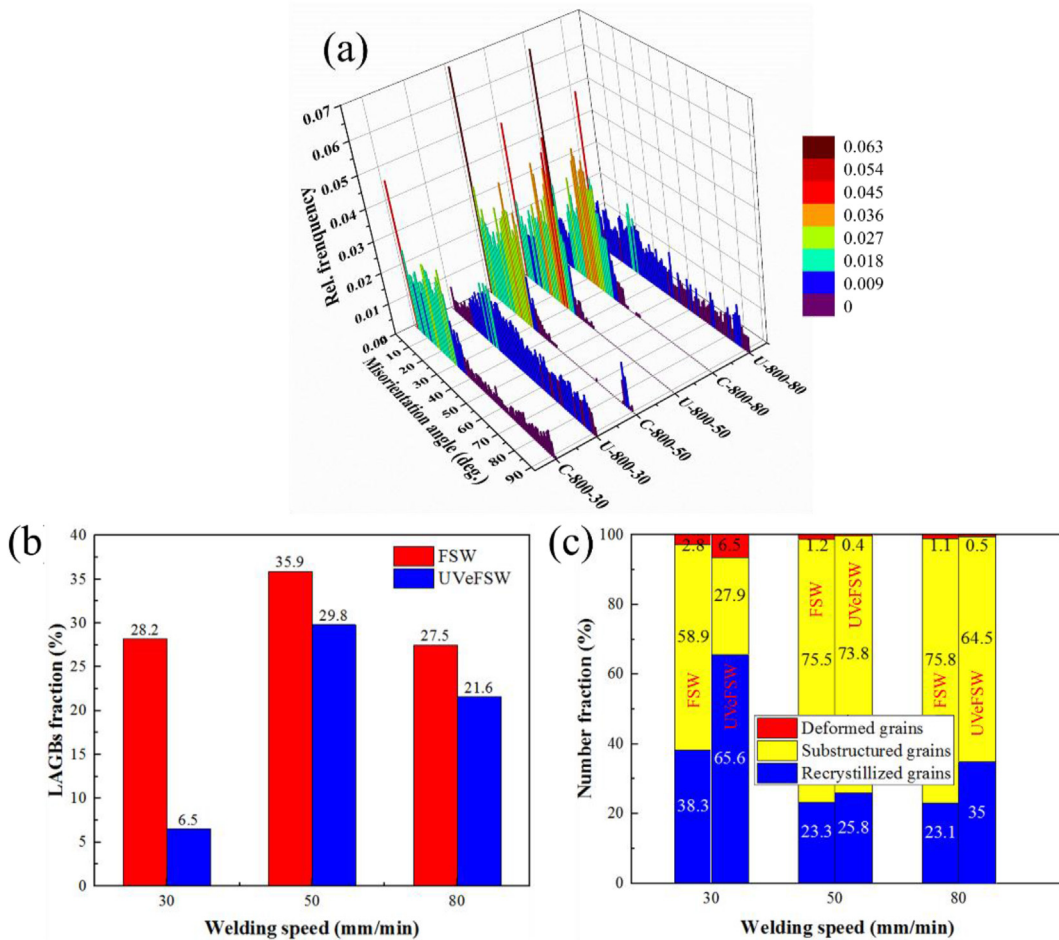


Fig. 8 – Grain microstructure information at location B3 (the WNZ in the Mg side) in FSW and UVeFSW. (a) Misorientation angle distribution, (b) LAGBs fraction, (c) Comparison of recrystallization degree.

application of UV, from 1.68 μm reduced to 0.93 μm . Moreover, it can be found from Fig. 8a and b that the LAGBs fraction decreased greatly with UV field. At the same time, the recrystallization process was greatly improved (Fig. 8c). However, such a significant UV effect was not found in other two cases (50 and 80 mm/min). FSW is a complex process with coupled thermal-mechanical-material flow behaviors, and the influence mechanism of UV field on the multi-field physical coupling needs to be further studied.

Some twin grains were found in case C-800-50, as shown by the white arrow in Fig. 7c. And it can also be seen from Fig. 8a that the misorientation angle has an obvious peak at about 86°. Similar phenomenon was also observed in FSW of Mg alloys by other scholars [36,39], and explained that this should be related to the transformation of twin boundary into HAGBs during large strain deformation. However, no twins were found in the weld of U-800-50. When the welding speed was 80 mm/min, the misorientation angle was mainly distributed in the range of 10–30°. With applied UV field, the misorientation angle was widely distributed in the range of 2–93°. This also occurred at the case of welding speed 30 mm/min. Mironov et al. [36] pointed out that when the misorientation angle was widely distributed between 15 and 93°, DDRX occurred. Therefore, in the FSW cases of C-800-30 and C-800-80, the

dominant recrystallization mechanism was CDRX, while in UVeFSW that was DDRX. In the CDRX process, a large amount of LAGBs are generated, and then these LAGBs gradually transform to HAGBs. However, in DDRX process, it does not need to produce a large amount of LAGBs to complete the recrystallization process. In addition, the higher degree of recrystallization means that more LAGBs have been transformed to HAGBs. That is why the LAGBs fraction decreases significantly when UV was applied at welding speed 30 mm/min.

Similarly, the dominant recrystallization mechanism of grains was CDRX in both C-800-50 and U-800-50. However, the twin recrystallization mechanisms also appeared in C-800-50. This illustrates that UV has an important effect on the recrystallization process of grains in the WNZ of the Mg side. Meanwhile, Fig. 8c shows that under the welding speed of 30 and 80 mm/min, the application of UV significantly improved the recrystallization degree of grains. In addition, it is worth noting that for both FSW and UVeFSW, there was a peak in the misorientation angle at about 30°. This is because the maximum rotation angle of grain orientation around the c-axis will not exceed 30° when Mg alloy grains recrystallize and grow, since Mg has hexagonal close-packed crystal structure [36,40,41].

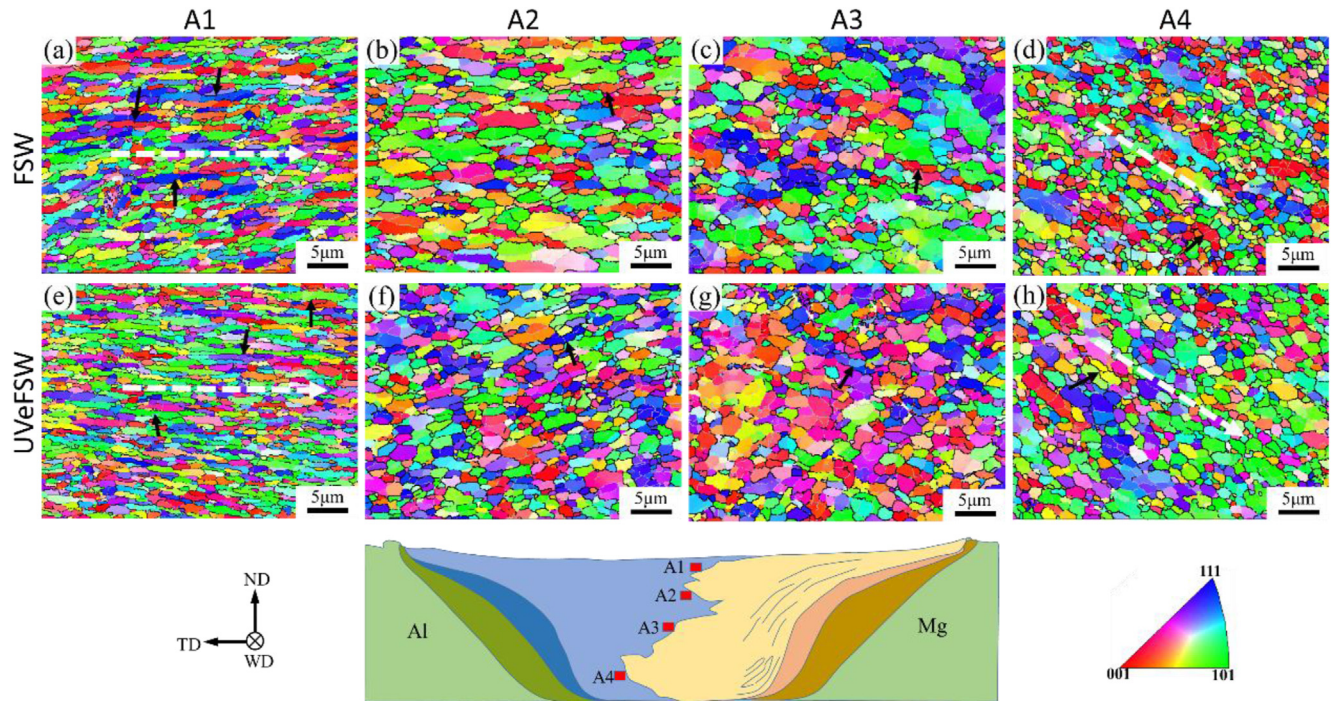


Fig. 9 – IPF maps of grain microstructures at locations A1-A4 (the WNZ in the Al side) in FSW and UVeFSW (welding speed 50 mm/min).

3.4. Variation of grain microstructure along weld depth direction

Since the shoulder has a big diameter than the pin, the material in the WNZ at different depths experiences different thermo-mechanical actions during the FSW process [42]. This uneven distribution of temperature and strain/strain rate along the thickness direction has an important impact on the microstructures of the weld [43]. Therefore, four different depth positions (A1-A4 and B1–B4 in Fig. 4g) were selected along the Al/Mg bonding interface to observe the grain microstructure.

3.4.1. Grain microstructure at A1-A4

In Al alloy side, the EBSD scanning positions were A1-A4 as shown in Fig. 4g. Fig. 9 presents the grain microstructures at four locations A1-A4 in FSW and UVeFSW welds made at welding speed of 50 mm/min (the joint was with the highest strength at this welding speed [23]). Since location A1 was only 0.5 mm below the top surface of the weld, the material here underwent severe plastic deformation due to the influence of the shoulder, and the grains were pulled into stripes with obvious deformation orientation in the horizontal direction, as shown by the white dotted line in Fig. 9a and e. Location A2 was a little far away from the shoulder, and was less affected by the shoulder, so that the grains here were only slightly elongated (Fig. 9b and f). The grains in regions A3 and A4, mainly affected by the pin, experienced relatively lower strain and strain rate, so that they were composed of equiaxed grains. However, the grains at region A4 had an obvious inclined downward deformation band (as shown by the white dotted lines in Fig. 9d and h), which was related to the local

material flow. Only in term of grain morphology, there was no obvious difference in FSW and UVeFSW. In addition, due to the influence of shoulder, the recrystallization process of grains in region A1 was greatly affected by strain. As shown by the black arrows in Fig. 9, many elongated grains were decomposed into several sub-grains with the same orientation, which shows that GDRX played an important role in region A1. However, this phenomenon was less obvious in regions A2-A4 where CDRX became the major recrystallization mechanism of grains.

According to statistics of grain size in Fig. 9, for FSW sample, the average grain size in regions A1-A4 was 0.67 ± 0.18 ; 0.91 ± 0.26 ; 1.18 ± 0.24 and $0.93 \pm 0.25 \mu\text{m}$, respectively. In UVeFSW, the average grain size was 0.62 ± 0.16 ; 0.96 ± 0.23 ; 0.98 ± 0.22 and $0.96 \pm 0.23 \mu\text{m}$, respectively. In both FSW and UVeFSW welds, the average grain size increased first and then decreased with the increase of the distance from the top surface of the weld, although the grain size difference is small. The minimum grain size appeared at the position close to the shoulder (region A1), while the maximum grain size occurred at the mid-depth of the weld (region A3). In addition, it is worth noting that there was almost no difference in the average grain size at locations A2, A3 and A4 in UVeFSW, but a significant size difference existed there in FSW. This should be due to the UV field induced variation of thermal-mechanical process in WNZ. When the UV field was applied, the average grain size at locations A1 and A3 decreased and increased at locations A2 and A4, but the difference in grain size was very small in FSW and UVeFSW of dissimilar Al/Mg alloys. Hu et al. [44] found the grain size in the WNZ of 2219-T6 Al alloy FSW increased after the application of UV field. Gao et al. [45] and Padhy et al. [30]

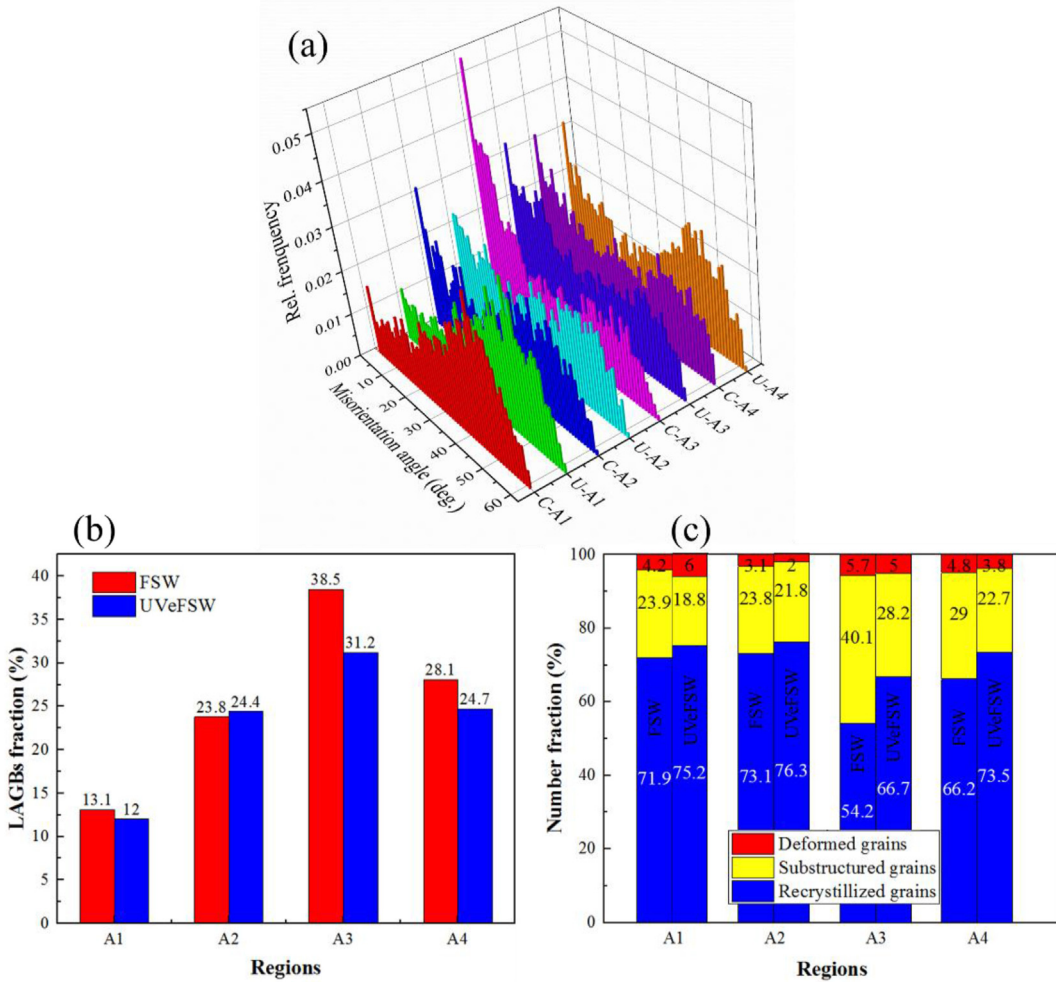


Fig. 10 – Grain microstructure information at locations A1-A4 in FSW and UVeFSW. (a) Misorientation angle distribution, (b) LAGBs fraction, (c) Comparison of recrystallization degree.

found that the grain size in the WNZ of 2024-T3 or 6061-T6 Al alloy FSW was refined after applying UV. Therefore, the UV effect on the grain microstructure evolution is more complicated in dissimilar FSW, and further study needs to be made in this aspect.

Fig. 10 shows the misorientation angle distribution, LAGBs fraction and recrystallization degree of grains in regions A1-A4. It is worth noting that the LAGBs fraction in regions A1-A4 increased first and then decreased (Fig. 10b), and the minimum value was found at region A1, but the recrystallization degree of grains at region A1 was not the largest, which was slightly lower than that in region A2 (Fig. 10c). This should be due to different mechanisms of grain recrystallization. In region A1, the grains were greatly affected by the strain in shoulder affected zone, GDRX was the main recrystallization mechanism, while other regions were less affected by shoulder, and CDRX was the main recrystallization mechanism. Therefore, the grains in region A1 did not need to gradually transform from LAGBs to HAGBs during the recrystallization process. Moreover, the misorientation angle in region A1 was mainly distributed in the high angle range (Fig. 10a). With application of UV field, although there was no obvious difference in the recrystallization mechanism and the misorientation angle

distribution in regions A1-A4, the degree of recrystallization has been improved to varying degrees (Fig. 10c).

3.4.2. Grain microstructures at B1–B4

Fig. 11 shows the grain microstructures at different depth positions (B1–B4 in Fig. 4g) in the WNZ of the Mg side. In region B1, the grains have obvious $\langle 0001 \rangle$ orientation, while for other locations, except region B4 in UVeFSW, most grains were close to $\langle 0001 \rangle$ orientation. This phenomenon is related to the fact that the material flow during welding is mainly affected by the shear force of the pin [38]. For the region B4 in UVeFSW, it is at the bottom of the WNZ. Generally, the Al/Mg material will be violently mixed here under the influence of the tip end of the pin [9,23,44]. Therefore, the flow of the material is more complex, and the grain orientation is no longer simply affected by the shear force of the pin. In addition, the grains in region B1 were equiaxed, which was different from that of Al alloy side where grains were elongated under the influence of shoulder. This should be due to the different stacking fault energy of Al and Mg, resulting in different recrystallization processes.

According to statistics of grain size in Fig. 11, the average grain size of regions B1–B4 in FSW was 1.41 ± 0.23 ; 1.64 ± 0.35 ;

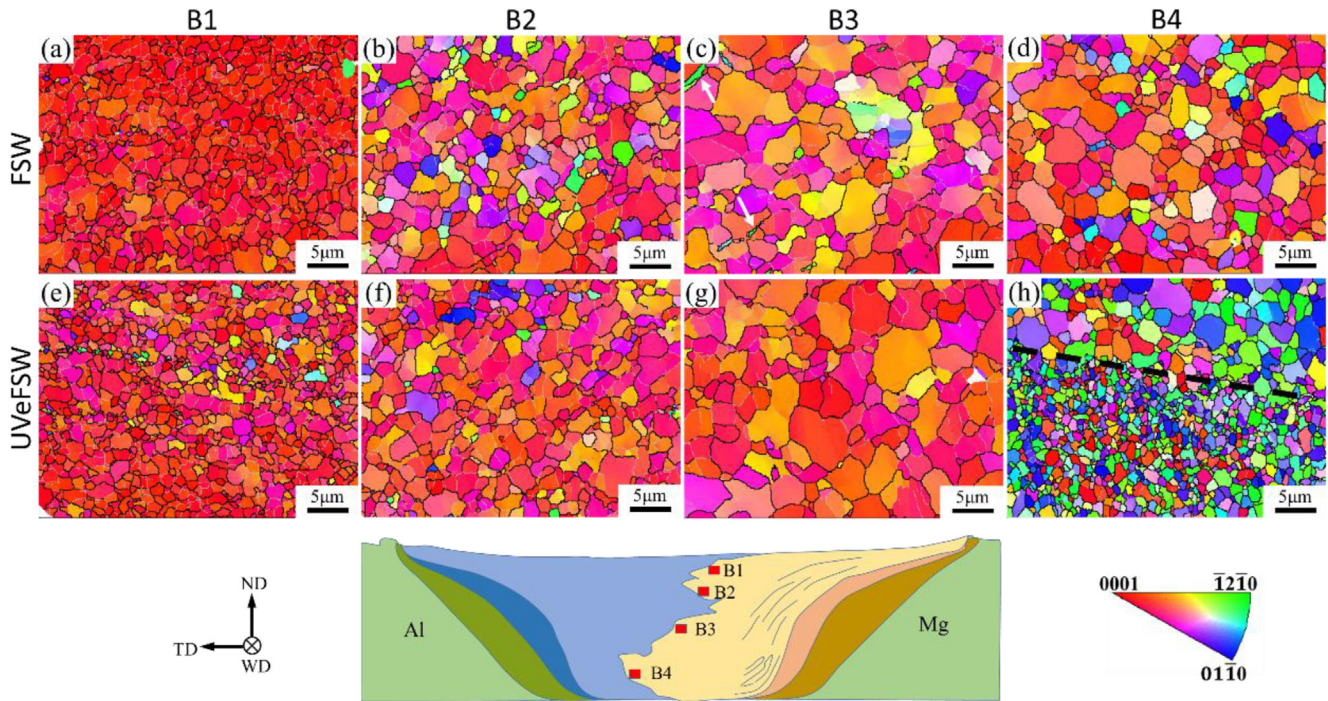


Fig. 11 – IPF maps of grain microstructures at B1–B4 (the WNZ in the Mg side) in FSW and UVeFSW (welding speed 50 mm/min).

2.57 ± 0.43 and 1.88 ± 0.31 μm , respectively. In UVeFSW, the average grain size at B1–B4 was 1.08 ± 0.22 ; 1.66 ± 0.38 ; 2.32 ± 0.44 and 0.92 ± 0.37 μm , respectively. The grain size in the Mg alloy side was larger than that in the Al alloy side. With the increase of the distance from the top surface of the weld, the average grain size in regions B1–B4 first increased and then decreased, and the maximum grain size was at the mid-depth of the weld (B3), like the case at the Al alloy side. With application of UV, the grain size in regions B1, B3 and B4 decreased, and only the grain size in region B2 increased slightly. And except for region B4, the differences in other regions are also very small like that in the Al alloy side.

Different from the Al alloy side, the smallest grain size at the Mg alloy side in UVeFSW did not appear in region B1, but in region B4. This was because region B4 contains fine grain area. As shown in Fig. 11h, it can be divided into coarse grain area and fine grain area according to grain size, and its boundary was roughly defined by the black dotted line. After statistics, the average grain size of coarse grain area and fine grain area was ~ 1.41 μm and ~ 0.82 μm , respectively. This demonstrates that the material here underwent ununiform plastic deformation. Region B4 locates in the severe mixing zone, so that the grain evolution at different points of this region is different. In this study, the EBSD scanning region was determined just according to the distance from the bottom of the weld. This also be the reason why the grain microstructure is so different between C–B4 and U–B4. Therefore, further experimental research is needed to understand the evolution process of grains in different locations at the bottom of the weld.

Fig. 12 shows the microstructure information of the grains at locations B1–B4 in FSW and UVeFSW. For regions B1–B3 in

both FSW and UVeFSW, the misorientation angle was mainly distributed at $2\text{--}30^\circ$, and there were peaks at about 2° and 30° . But the grain misorientation angle in region B4 was widely distributed at $2\text{--}90^\circ$, and there was a peak only at about 30° . The reason for this difference may be that the dominant recrystallization mechanism is different [36], that is, the dominant mechanism in region B1–B3 is CDRX, while in region B4 it is DDRX. There was also an obvious peak at about 86° in region B3 in FSW. This is because twin grains appeared at region B3 in FSW, as shown by the white arrow in Fig. 11c. There was no obvious difference between FSW and UVeFSW in the misorientation angle distribution in other regions.

According to statistics, the LAGBs fraction in region B4 was the lowest, which was 11.7% in FSW and 8.1% in UVeFSW (Fig. 12b). On one hand, this is due to the high degree of recrystallization in this region (Fig. 12c), on the other hand, DDRX does not produce a large amount of LAGBs. The regions B1–B3 contained a large amount of LAGBs. The LAGBs in region B1 was the largest in FSW, while in UVeFSW the LAGBs in region B2 was the largest. Moreover, with application of UV field, the LAGBs in region B2 increased, but the recrystallization degree of grains in each region was improved to varying degrees. This is because that UV not only promotes the grain recrystallization process, but also affects the grain recrystallization mechanism. That is, the area fraction of grains with CDRX or DDRX changes. It can be concluded that although the grains in the Mg alloy side and the Al alloy side experienced almost similar thermal–mechanical processes during the welding, there were different evolution regularities of grain microstructures at both sides along the weld depth direction due to the different stacking fault energy and initial grain size of base materials.

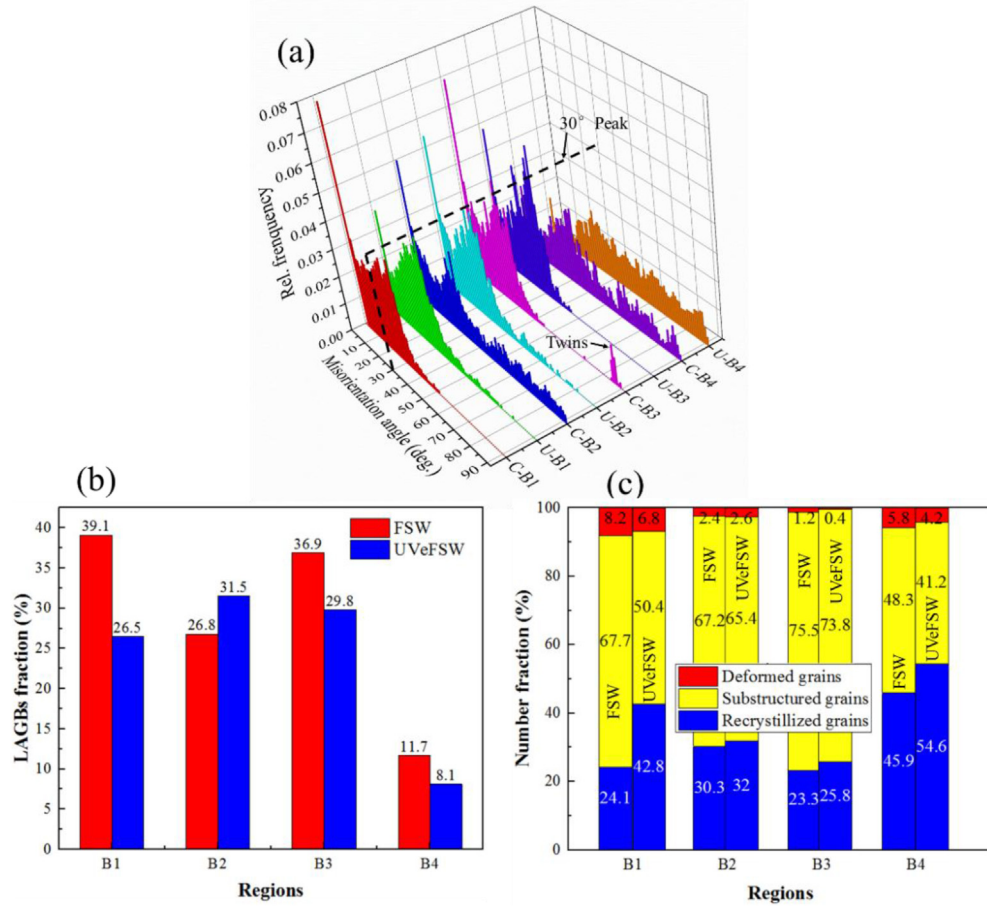


Fig. 12 – Grain microstructure information in B1–B4 of FSW and UVeFSW, (a) Misorientation angle distribution, (b) LAGBs fraction, (c) Comparison of recrystallization degree.

3.5. Grain microstructure in the TMAZ

To better understand the ultrasonic influence on the changes of grain structures in different regions of the weld, the grains in thermal mechanical affected zone (TMAZ) were characterized and analyzed.

Fig. 13 shows the grain microstructure information at location A5 (Fig. 4g) in the TMAZ of the Al alloy side. It should be noted that because UV caused expansion of the WNZ volume in UVeFSW [10,23,44], the selected checking point A5 in UVeFSW was a little bit farther from the weld centerline than that in FSW, as indicated in Fig. 4g. There were large grains and fine grains at location A5 in the TMAZ of the Al alloy side, and the fine grains were mainly distributed at boundaries of large grains, formed a typical necklace structure (Fig. 13a and c). From the grain boundaries images (Fig. 13b and f), it can be seen that a large amount of LAGBs were formed in the TMAZ of the Al alloy side. Its proportion in FSW and UVeFSW was 72.7% and 68.4%, respectively. In the welding process, although the material here did not directly contact with the tool, plastic deformation still occurred under the driving of the material flow in the stirred zone, resulted in a lot of dislocations generated in grains. And these dislocations formed LAGBs through aggregation and rearrangement. Simultaneously, dislocations

would accumulate here first because of the high distortion energy at the original grain boundaries.

Fig. 13d and h are KAM (kernel average misorientation) images, which were plotted with the average value of the orientation deviation between each pixel and the nearest pixel. It can be used to qualitatively indicate the uniformity of the plastic deformation of the material, and indirectly indicate the dislocation density of the material [46]. The higher KAM value indicates that it has larger strain and higher dislocation density. In Fig. 13d and h, the grain boundaries have higher KAM values, indicating the accumulated dislocations here. Under continuous action of deformation and heat, the LAGBs can transform to the HAGBs by absorbing and consuming dislocations, thereby formed new grains on original grain boundaries. This is a typical CDRX process, and this process would significantly reduce the dislocation density. As shown in Fig. 13, the grains in the area marked by the black circles or ellipses had completed recrystallization process, and thus had a lower dislocation density. When the UV field was applied, although there was not much difference in the morphology of the grain structures here, the degree of recrystallization was improved.

Fig. 14 shows the grain microstructure information at location B5 (Fig. 4g) in the TMAZ of the Mg alloy side. The

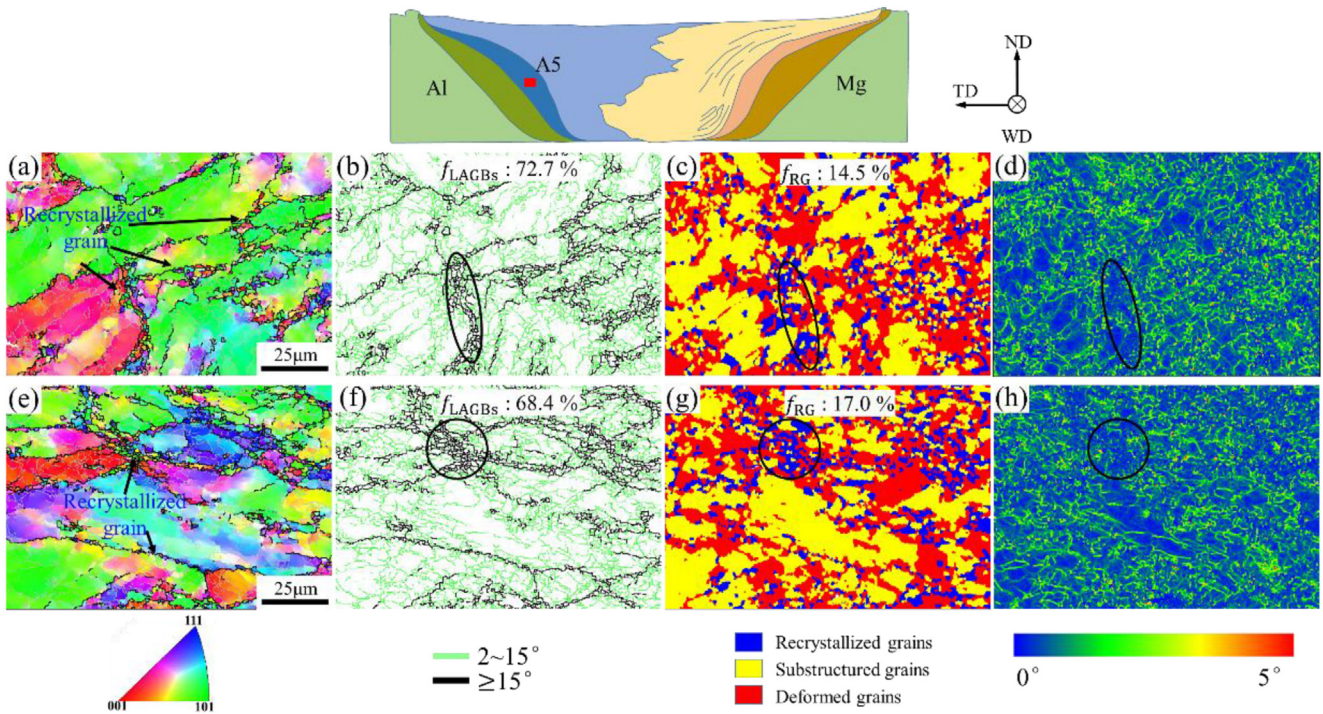


Fig. 13 – IPF maps (a,e), GB maps (b,f), grain morphology maps (c,g) and KAM maps (d,h) at A5 in Al side TMAZ (50 mm/min). (a, b, c, d): FSW; (e, f, g, h): UVeFSW.

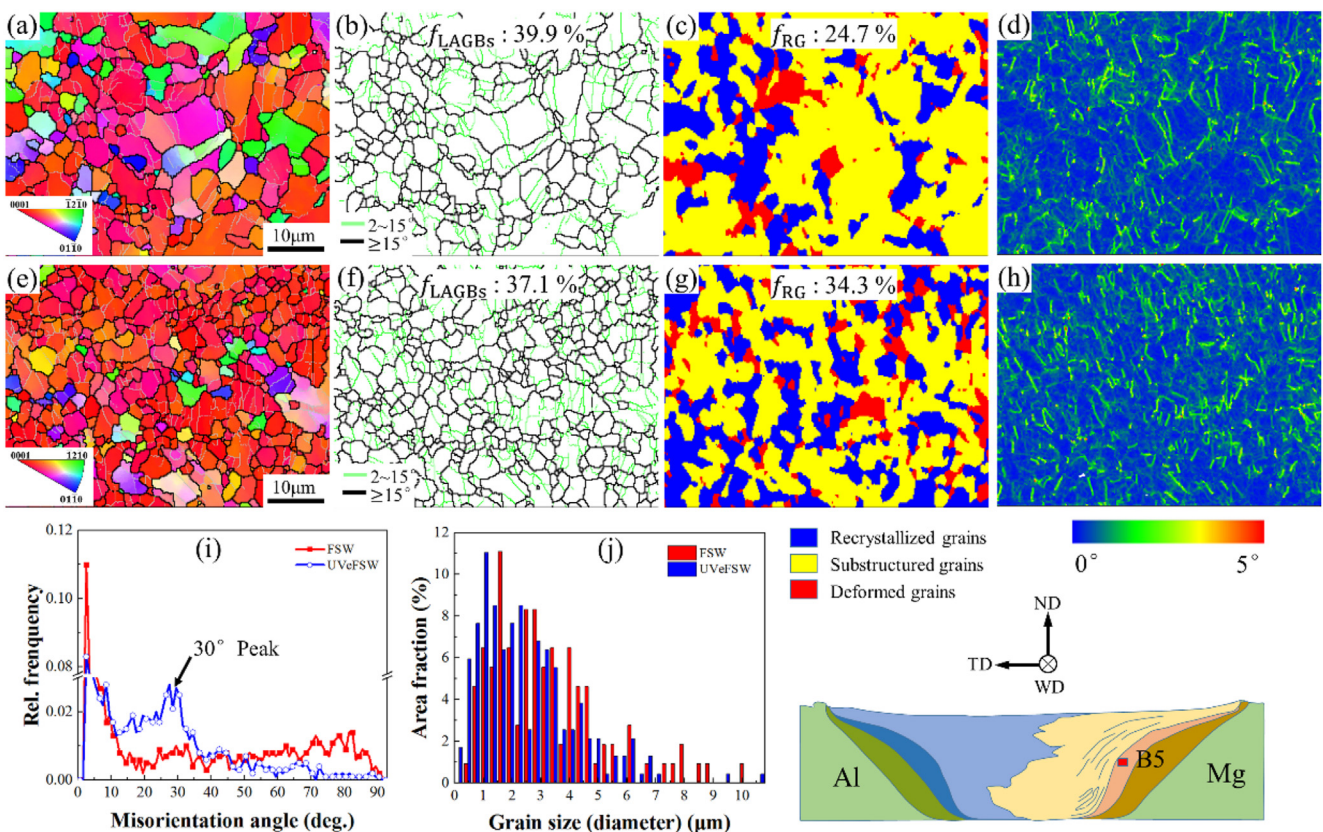


Fig. 14 – IPF maps (a,e), GB maps (b,f), grain morphology maps (c,g), KAM maps (d,h), misorientation angle distribution (i) and calculated grain size (j) at B5 in Mg side TMAZ (50 mm/min). (a, b, c, d): FSW; (e, f, g, h): UVeFSW.

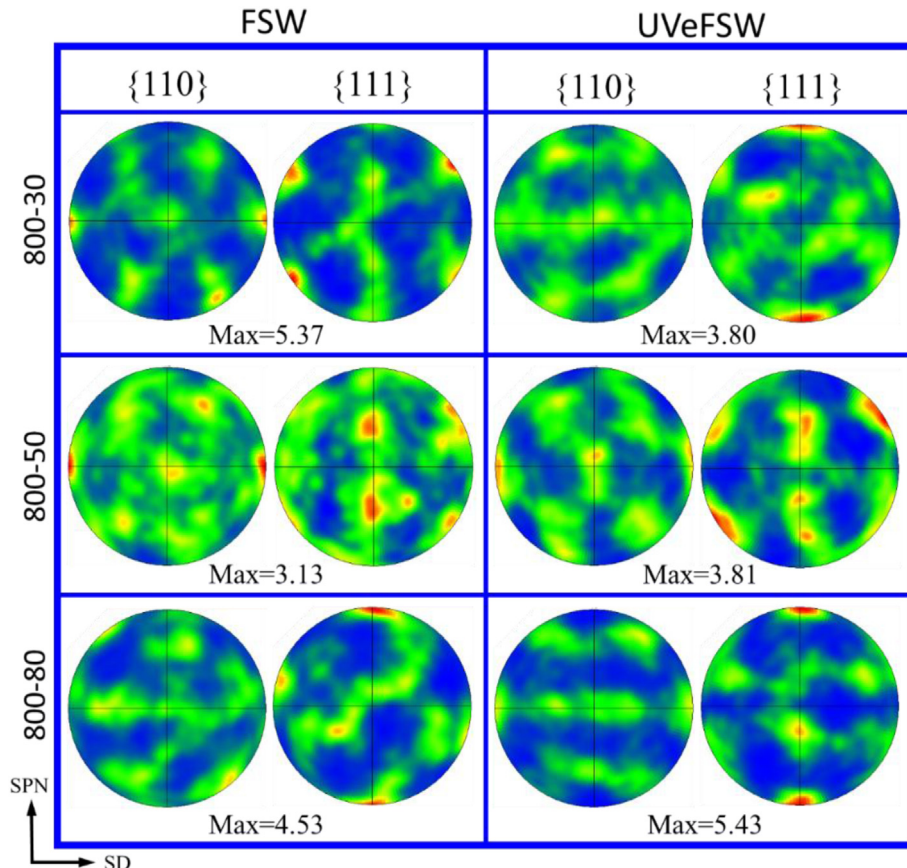


Fig. 15 – {101} and {111} pole figures at location A3 (the WNZ in the Al side) under different weld speeds. SPN-shear plane normal, SD-shear direction.

difference from the Al side was that the grain size here was relatively uniform. Meanwhile, Fig. 14c and g demonstrate that the grains in the TMAZ of the Mg alloy side have higher degree of recrystallization than that in Al side. There may be two reasons for this difference. First, in this study, Mg alloy was placed on the AS, so that it experienced more severe plastic deformation. Second, the Al alloy and Mg alloy have different stacking fault energy and deformability, so that the conditions for occurring recrystallization were different.

According to statistics of grain size in Fig. 14, the average grain size at the TMAZ of the Mg alloy side in FSW and UVeFSW was 3.34 ± 0.52 and $2.51 \pm 0.42 \mu\text{m}$, respectively. Obviously, the grains were refined when the UV was applied, which should be due to the recrystallization process promoted by UV field. In addition, the misorientation angle in FSW had a higher peak value at low angles ($2\text{--}5^\circ$), and had a wide distribution in the range of $20\text{--}90^\circ$, as shown in Fig. 14i. In UVeFSW, the grain misorientation angle was mainly distributed in the range of $2\text{--}30^\circ$, and had an obvious peak at about 30° . Mg base material contains large grains and small grains. These small grains would not undergo recrystallization under insufficient heat, so that some small grains may retained in the FSW. However, when the UV field was applied, the deformation degree of material increased, and the recrystallization degree increased, so that the original grains were replaced by recrystallized ones. Therefore, the misorientation angle distribution in FSW and UVeFSW was different.

3.6. Texture evolution

3.6.1. Al alloy side

During the welding process, the Al alloy material will arise preferred orientation during the grain growth process due to

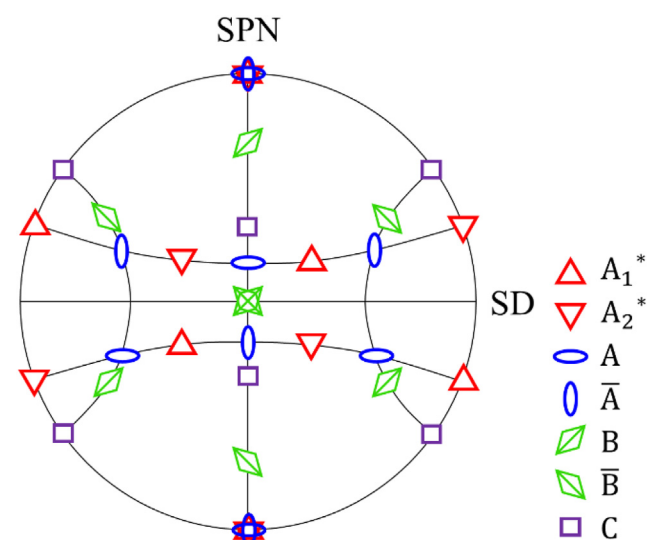


Fig. 16 – The standard {111} pole figure of FCC metals under simple shear. SPN-shear plane normal, SD-shear direction.

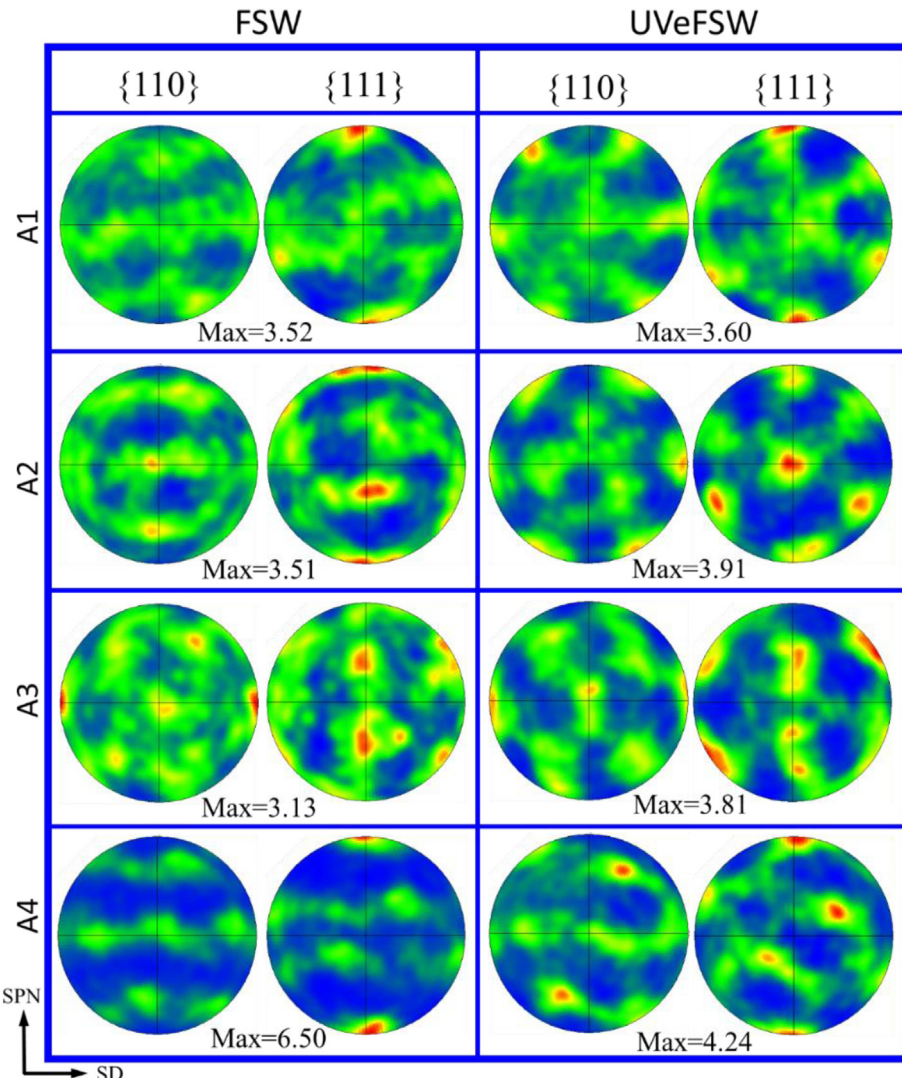


Fig. 17 – {101} and {111} pole figures at locations A1-A4 (the WNZ in the Al side, 50 mm/min).

the shearing and extrusion of the pin, and then form textures in WNZ. Fig. 15 shows the pole figures at location A3 in the WNZ of the Al side at different welding speeds after proper deflection. By compared with the {111} standard pole figure in the simple shear deformation of face-centered cubic metal (Fig. 16) [39], it can found that the texture component in C-800-30 was mainly $C\{001\}<110>$ shear texture, while the texture component in U-800-30 was mainly $A_1^*/A_2^*\{111\}<112>$ and $A/\bar{A}\{111\}<110>$ shear texture. When the welding speed was 50 and 80 mm/min, the main texture components in FSW and UVeFSW were same. At 50 mm/min, it is mainly composed of $C\{001\}<110>$ component, and at 80 mm/min, it was mainly composed of $A_1^*/A_2^*\{111\}<112>$ and $A/\bar{A}\{111\}<110>$ components. For different welding speeds, the texture component produced in the weld was different. In addition, when the welding speed was 30 mm/min, the maximum intensity of the texture was reduced with the application of UV field, from 5.37 MRD (multiple of random density) to 3.80 MRD. This may be related to the appearance of different shear textures. However, when the welding speed was 50 and 80 mm/min, the

maximum intensity was increased, because the UV enhanced the material deformation in the WNZ.

Fig. 17 shows the {110} and {111} pole figures at locations A1-A4 at Al side WNZ (welding speed 50 mm/min), and for the convenience to make comparison, they were also properly deflected. In FSW, the main texture components in locations A1, A2, and A4 were A_1^*/A_2^* and A/\bar{A} , and in location A3 was C component. In UVeFSW, the textures in location A1 was A_1^*/A_2^* and C components, in location A2 was B/\bar{B} components, in location A3 was C component, and in region A4 was A_1^*/A_2^* components. Except for the location A4, the texture intensity of other locations increased slightly when UV field was applied.

It is worth noting that the B/\bar{B} and C components are common textures in FSW of similar Al alloy [47,48]. But in this study, the B/\bar{B} component only appeared in location A2 in UVeFSW, and there were also fewer locations where C texture appeared. The texture components A_1^*, A_2^*, A and \bar{A} usually occur in the deformation process with lower strain, while the B/\bar{B} and C components appear with higher strain

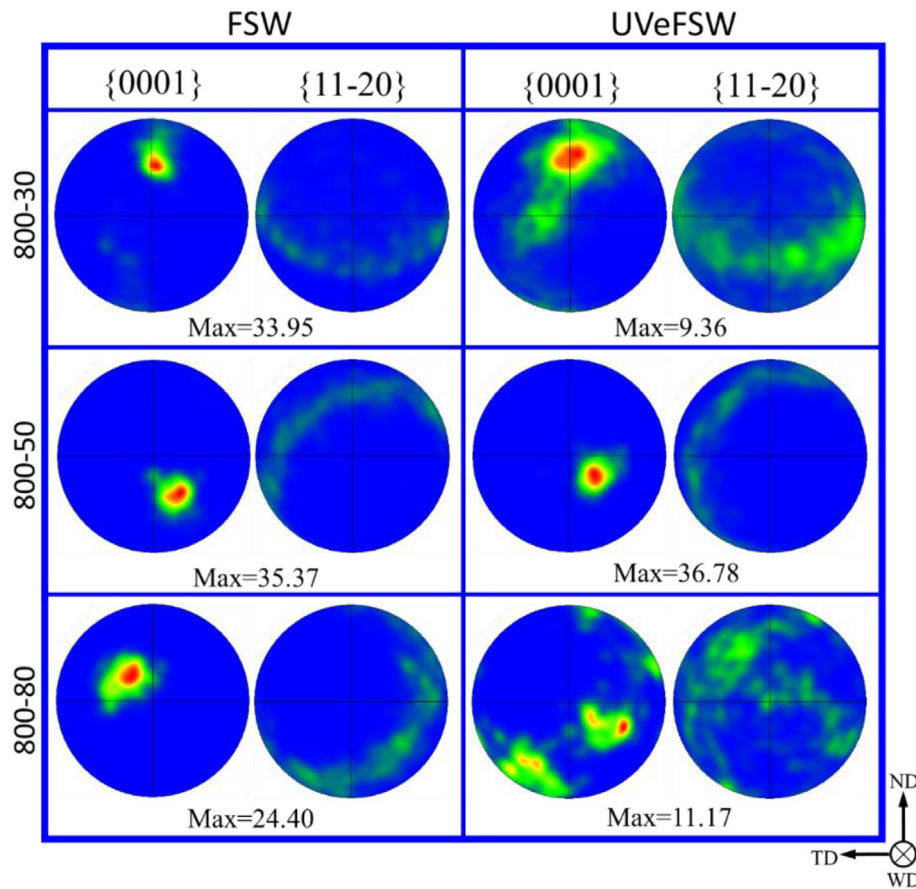


Fig. 18 – {0001} and {11-20} pole figures at location B3 (the WNZ in the Mg side) under different weld speeds.

deformation. And the appearance of B/\bar{B} texture requires the material to experience greater strain than C texture [47]. Therefore, from the texture components it was found that the degree of material deformation in Al/Mg dissimilar FSW is relatively low. However, the WNZ in UVeFSW contains more B/\bar{B} and C shear textures, which indicates that the strain of the material in WNZ was increased when the UV was applied. This proves that the UV can promote the plastic deformation and material flow in the WNZ in terms of texture evolution.

3.6.2. Mg alloy side

Fig. 18 shows the {0001} and {11-20} pole figures at location B3 in the WNZ of the Mg alloy side at different welding speeds. It can be found that the {0001} base texture was mainly produced in the WNZ of the Mg alloy side. This is the same as the texture component commonly found in FSW of same Mg alloy [37,39].

In FSW, the grains deformation is mainly driven by the shear action of the pin, and the direction of the shear force is the tangent direction of the pin surface. Thus, the grain c-axis in the central area of the WNZ is generally parallel to the welding direction (WD) [38]. However, in this study, the c-axis of grains was deviated. There are two reasons for this phenomenon. First, in this study, although the EBSD scanning area was located 1.5 mm from the bottom of the weld (the mid-depth), it would be slightly biased to the Al side or Mg side because the Al/Mg bonding interface was tortuous and irregular. Second, the pin used in this study was cone-shaped, so

that the normal direction of shear force at the weld center was not parallel to WD. However, when the welding speed was 30 mm/min, the grain c-axis deflected to ND in both FSW and UVeFSW. Considering the obvious downward trend of material flow at 30 mm/min (Fig. 5a and b), the deflection of the c-axis here may be caused by the downward flow of the material. In addition, the texture intensity was significantly reduced when UV field was applied at welding speed of 30 and 80 mm/min. This is because more complete recrystallization behavior of Mg alloy grains occurred in UVeFSW, which weakened the orientation of grains.

The {0001} and {11-20} pole figures at different depth positions in the WNZ of the Mg alloy side are shown in Fig. 19. Although the locations in the weld were different, the {0001} base texture all formed. Firstly, in locations B1–B3, regardless of FSW or UVeFSW, the grain c-axis was approximately parallel to WD, which was the result of the shear force effect of the pin during material deformation [38]. However, in location B4, not only the grain c-axis deflected greatly, but also the texture intensity decreased significantly. As mentioned earlier, the materials at B4 located in the severe deformation zone, and the material flow in this zone is not simply horizontal or vertical but like swirl [9,23,44], so that the preferred orientation during grain growth was also changed. Meanwhile, the higher degree of recrystallization in this location (Fig. 12c) would weaken the preferred orientation of grain growth. In addition, Mironov et al. [36] pointed out that a

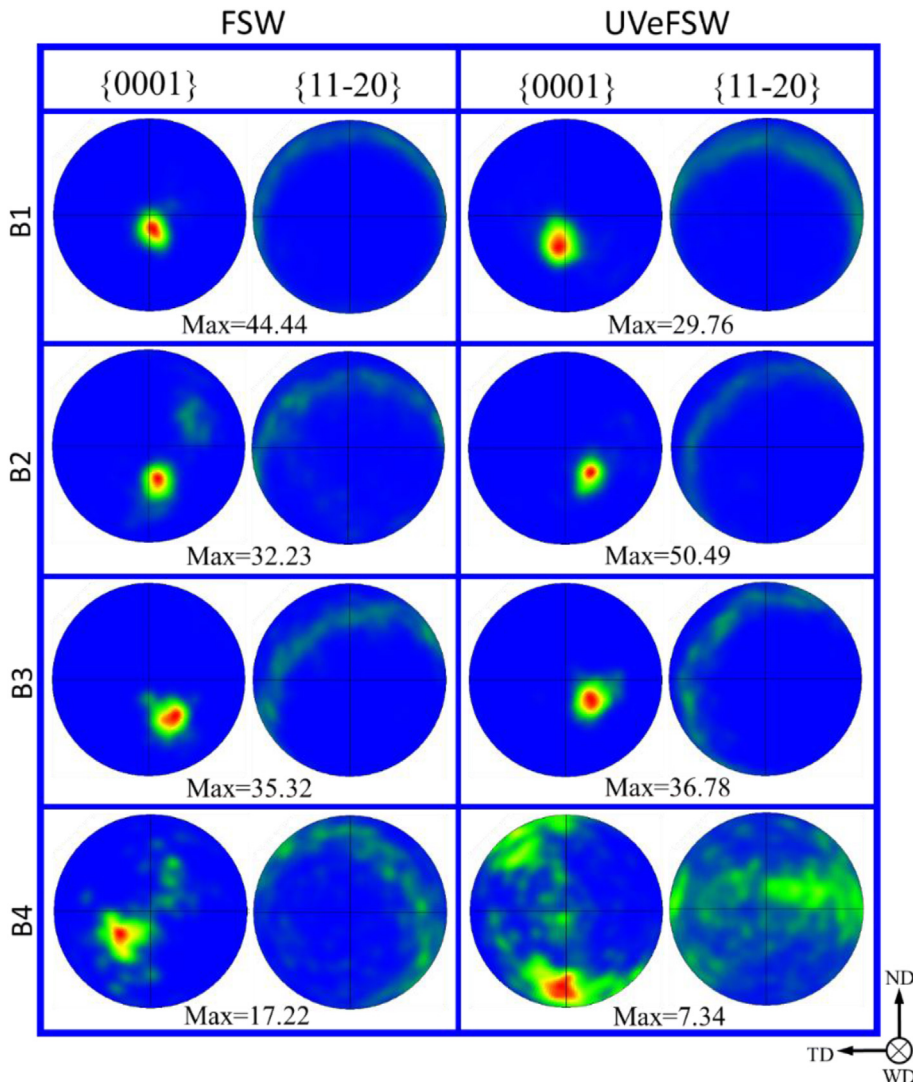


Fig. 19 – {0001} and {11-20} pole figures at locations B1–B4 (the WNZ in the Mg side, 50 mm/min).

strong basal texture would be formed when the grain misorientation angle was almost not distributed between 30 and 85°. The misorientation angle distribution (Figs. 8 and 12) and the pole figures (Figs. 18 and 19) in this study are consistent with the result in [36].

3.7. Role of UV field

Based on the grain microstructure at different locations under different welding speeds, a common characteristic was found. That is, regardless of how the grain size changed with and without application of UV, the degree of grains recrystallization was always improved. During the welding process, the Al/Mg material flows from the front to the back of the pin under the shearing and squeezing action of the tool, and finally deposits behind the tool and fills the gap left by the pin. During this high temperature and high strain process, the grains undergo dynamic recrystallization behavior. Although the grain microstructure in Al and Mg side weld has different recrystallization processes, they all depend on the motion of dislocations and

the migration or slippage of grain boundaries. It is well known that UV can promote the motion of dislocations in metal plastic processing [35,44,49,50]. Essentially, friction stir welding is also a metal plastic deformation process. Thereby, the UV in FSW can promote the motion of dislocations, and then promote the entanglement, aggregation, rearrangement of dislocations and the dipole annihilation. As shown in Fig. 20, during the dynamic recrystallization process, due to the influence of the UV, the motion and rearrangement of dislocations are accelerated. These continuously accumulating dislocations promote the formation of LAGBs, and at the same time, the transformation of LAGBs into HAGBs by absorbing dislocations is also accelerated. Thus, the degree of recrystallization of grains is increased. In this process, dislocations are also consumed in large quantities.

In general, the higher the degree of recrystallization, the smaller the grain size. This is also the reason why the average grain size decreased when UV field was applied in most sub-regions of WNZ. However, the role of UV in promoting dislocation motion and grain boundary transformation shortened

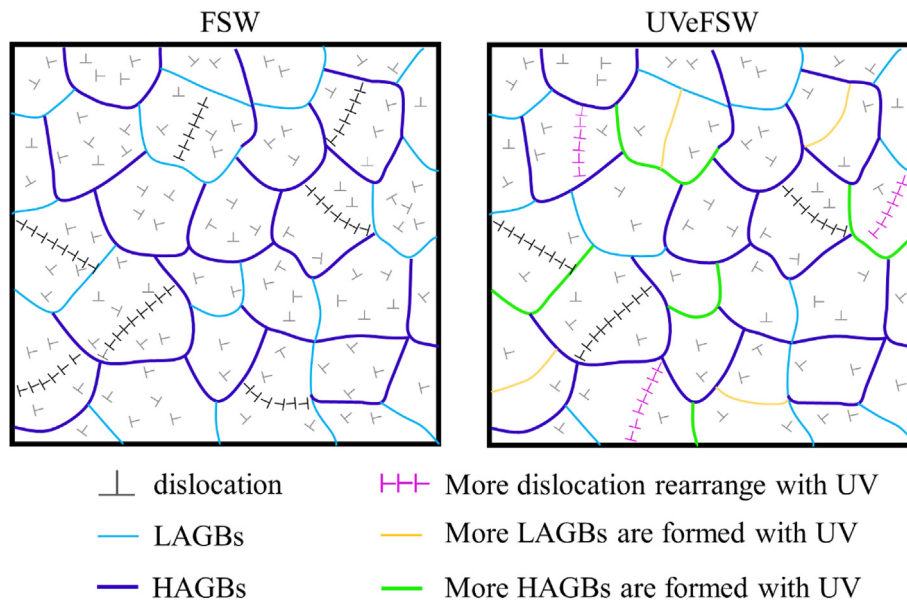


Fig. 20 – Schematic diagram of UV promotes dislocation motion and grain boundary formation.

the incubation period of recrystallized grain nucleation, which made the recrystallized grains enter the growth stage earlier. Meanwhile, UV can also promote grain boundary slip/migration. The applied UV can also promote generating a large number of vacancies by reducing the vacancy formation energy [44]. These vacancies are easy to deposit at the grain boundary under the lowest energy criterion, which can not only promote the motion of dislocations at the grain boundary, but also promote the self-diffusion of the grain boundary [51]. Thus, grain boundary slip or migration are also indirectly promoted. This causes the recrystallized grains nucleate earlier and grow faster in UVeFSW, leading to an increase in the average grain size in some locations. A typical example was in Al side WNZ of C-800-80, as shown in Fig. 5e and f. Although the recrystallization degree of grains in conventional FSW was low, it contained a large number of fine recrystallized grains that had not yet grown, so that the average grain size was smaller than that in UVeFSW. In addition, the acoustic softening effect of UV can promote the material flow in the WNZ, which also has a certain impact on the recrystallization mechanism of grains.

4. Conclusions

- (1) In dissimilar FSW of Al/Mg alloys, the recrystallization mechanisms of WNZ grains at Al alloy side are CDRX and GDRX, while at Mg alloy side, that are CDRX and DDRX. In both sides, CDRX plays a leading role. Compared with the cases in FSW of same alloys, finer grains structures were obtained in dissimilar FSW of Al/Mg alloys due to a little bit lower welding temperature.
- (2) Ultrasonic vibration has little influence on the recrystallization mechanism of grains at Al alloy side, but has

great effect on the grains structure in the Mg alloy side. Especially when the welding speed was 30 and 80 mm/min, the exerted ultrasonic vibration changed the main recrystallization mechanism of grains in the Mg alloy side, that is, from CDRX to DDRX.

- (3) Although there are different grain evolution processes at Al alloy and Mg alloy sides, their average grain sizes in WNZ increased first and then decreased with increasing of welding speed. The average grain sizes in the WNZ also increased first and then decreased along the thickness direction, and the maximum grain size was at the mid-depth of the weld.
- (4) For joining of dissimilar Al/Mg alloys, low strain shear texture appeared more in the WNZ of the Al side, such as A_1^* , A_2^* , A and \bar{A} components in FSW, while in UVeFSW, more regions in the WNZ were with high strain shear textures C and B/\bar{B} , because the acoustic softening effect of ultrasonic field promoted the material deformation. In the WNZ of the Mg side, only $\{0001\}$ basal texture appeared in both FSW and UVeFSW.
- (5) Ultrasonic vibration can promote the motion, aggregation and annihilation of dislocations in stirred zone, which is the key factor affecting the thermal-mechanical behavior in the welding process. Thus, the evolution of grain microstructure in the weld was varied, and the recrystallization degree of grains was improved in UVeFSW.

Declaration of Competing Interest

The authors declare that they have no known competing financial interests or personal relationships that could have appeared to influence the work reported in this paper.

Acknowledgement

The authors appreciate the financial support to this work from the National Natural Science Foundation of China (Grant No. 52035005).

REFERENCES

- [1] Shah LH, Othman NH, Gerlich A. Review of research progress on aluminium-magnesium dissimilar friction stir welding. *Sci Technol Weld Join* 2018;23:256–70.
- [2] Firouzdor V, Kou S. Al-to-Mg friction stir welding: effect of material position, travel speed, and rotation speed. *Metall Mater Trans A* 2010;41:2914–35.
- [3] Ma ZY. Friction stir processing technology: a review. *Metall Mater Trans A* 2008;39:642–58.
- [4] Chen K, Liu X, Ni J. A review of friction stir-based processes for joining dissimilar materials. *Int J Adv Manuf Technol* 2019;104:1709–31.
- [5] Prangnell PB, Heason CP. Grain structure formation during friction stir welding observed by the 'stop action' technique. *Acta Mater* 2005;53:3179–92.
- [6] Yu PF, Wu CS, Shi L. Analysis and characterization of dynamic recrystallization and grain structure evolution in friction stir welding of aluminum plates. *Acta Mater* 2021;207:116692.
- [7] Fonda RW, Bingert JF, Colligan KJ. Development of grain structure during friction stir welding. *Scripta Mater* 2004;51:243–8.
- [8] Heidarzadeh A, Mironov S, Kaibyshev R, Çam G, Simar A, Gerlich A, et al. Friction stir welding/processing of metals and alloys: a comprehensive review on microstructural evolution. *Prog Mater Sci* 2020;117:100752.
- [9] Liang ZY, Chen K, Wang XN, Yao JS, Yang Q, Zhang LT, et al. Effect of tool offset and tool rotational speed on enhancing mechanical property of Al/Mg dissimilar fsw joints. *Metall Mater Trans A* 2013;44:3721–31.
- [10] Lv X, Wu CS, Yang C, Padhy GK. Weld microstructure and mechanical properties in ultrasonic enhanced friction stir welding of Al alloy to Mg alloy. *J Mater Process Technol* 2018;254:145–57.
- [11] Xie Y, Meng X, Li Y, Mao D, Wan L, Huang Y. Insight into ultra-refined grains of aluminum matrix composites via deformation-driven metallurgy. *Compos Commun* 2021;26:100776.
- [12] Xie Y, Meng X, Wang F, Jiang Y, Ma X, Wan L. Insight on corrosion behavior of friction stir welded AA2219/AA2195 joints in astronautical engineering. *Corrosion Sci* 2021;192:109800.
- [13] Meng X, Huang Y, Cao J, Shen J, Santos JFD. Recent progress on control strategies for inherent issues in friction stir welding. *Prog Mater Sci* 2020;115:100706.
- [14] Zhao Y, Lu Z, Yan K, Huang L. Microstructural characterizations and mechanical properties in underwater friction stir welding of aluminum and magnesium dissimilar alloys. *Mater Des* 2015;65:675–81.
- [15] Mofid MA, Abdollah-Zadeh A, Ghaini FM, Gür CH. Submerged friction-stir welding (SFSW) underwater and under liquid nitrogen: an improved method to join Al alloys to Mg alloys. *Metall Mater Trans A* 2012;43:5106–14.
- [16] Mehta KP, Carbone P, Astarita A, Scherillo F, Rubino F, Vora P. Conventional and cooling assisted friction stir welding of AA6061 and AZ31B alloys. *Mater Sci Eng, A* 2019;759:252–61.
- [17] Bilgin M, Karabulut S, Özdemir A. Investigation of heat-assisted dissimilar friction stir welding of AA7075-T6 aluminum and AZ31B magnesium alloys. *J Sci Eng* 2020;45:1081–95.
- [18] Chang WS, Rajesh SR, Chun CK, Kim HJ. Microstructure and mechanical properties of hybrid laser-friction stir welding between AA6061-T6 Al Alloy and AZ31 Mg Alloy. *J Mater Sci Technol* 2011;27:199–204.
- [19] Benfer S, Straß B, Wagner G, Fürbeth W. Manufacturing and corrosion properties of ultrasound supported friction stir welded Al/Mg-hybrid joints. *Surf Interface Anal* 2016;48:843–52.
- [20] Ji S, Meng X, Liu Z, Huang R, Li Z. Dissimilar friction stir welding of 6061 aluminum alloy and AZ31 magnesium alloy assisted with ultrasonic. *Mater Lett* 2017;201:173–6.
- [21] Liu Z, Meng X, Ji S, Li Z, Wang L. Improving tensile properties of Al/Mg joint by smashing intermetallic compounds via ultrasonic-assisted stationary shoulder friction stir welding. *J Manuf Process* 2018;31:552–9.
- [22] Liu X, Wu CS, Padhy GK. Characterization of plastic deformation and material flow in ultrasonic vibration enhanced friction stir welding. *Scripta Mater* 2015;102:95–8.
- [23] Zhao J, Wu CS, Su H. Acoustic effect on the tensile properties and metallurgical structures of dissimilar friction stir welding joints of Al/Mg alloys. *J Manuf Process* 2021;65:328–41.
- [24] Kumar S, Wu CS, Gao S. Process parametric dependency of axial downward force and macro- and microstructural morphologies in ultrasonically assisted friction stir welding of Al/Mg alloys. *Metall Mater Trans A* 2020;51:2863–81.
- [25] Lv XQ, Wu CS, Padhy GK. Diminishing intermetallic compound layer in ultrasonic vibration enhanced friction stir welding of aluminum alloy to magnesium alloy. *Mater Lett* 2017;203:81–4.
- [26] Peng P, Wang W, Jin Y, Liu Q, Zhang T, Qiao K, et al. Experimental investigation on fatigue crack initiation and propagation mechanism of friction stir lap welded dissimilar joints of magnesium and aluminum alloys. *Mater Char* 2021;177:111176.
- [27] Sun Z, Wu CS. A numerical model of pin thread effect on material flow and heat generation in shear layer during friction stir welding. *J Manuf Process* 2018;36:10–21.
- [28] Imandoust A, Barrett CD, Oppedal AL, Whittington WR, Paudel Y, Kadiri ElH. Nucleation and preferential growth mechanism of recrystallization texture in high purity binary magnesium-rare earth alloys. *Acta Mater* 2017;138:27–41.
- [29] Hu Y, Liu HJ, Li DR. Contribution of ultrasonic to microstructure and mechanical properties of tilt probe penetrating friction stir welded joint. *J Mater Sci Technol* 2021;85:205–17.
- [30] Padhy GK, Wu CS, Gao S. Precursor ultrasonic effect on grain structure development of AA6061-T6 friction stir weld. *Mater Des* 2016;116:207–18.
- [31] Watanabe H, Tsutsui H, Mukai T, Ishikawa K, Okanda Y, Kohzu M, et al. High-strain-rate superplasticity in an AZ91 magnesium alloy processed by ingot metallurgy route. *Mater Trans* 2001;42:1200–5.
- [32] Commin L, Dumont M, Masse JE, Barrallier L. Friction stir welding of AZ31 magnesium alloy rolled sheets: influence of processing parameters. *Acta Mater* 2009;57:326–34.
- [33] Chang CI, Lee CJ, Huang JC. Relationship between grain size and Zener–Holloman parameter during friction stir processing in AZ31 Mg alloys. *Scripta Mater* 2004;51:509–14.
- [34] Zhou H, Cui H, Qin QH. Influence of ultrasonic vibration on the plasticity of metals during compression process. *J Mater Process Technol* 2017;251:146–59.

- [35] Mao Q, Coutris N, Rack H, Fadel G, Gibert J. Investigating ultrasound-induced acoustic softening in aluminum and its alloys. *Ultrasonics* 2020;102:106005.
- [36] Mironov S, Onuma T, Sato YS, Kokawa H. Microstructure evolution during friction-stir welding of AZ31 magnesium alloy. *Acta Mater* 2015;100:301–12.
- [37] Zhou M, Sun Y, Morisada Y, Ushioda K, Fujii H. Quasi-in-situ investigation into the microstructure and texture evolution of pure magnesium during friction stir welding. *J Magnes Alloy* 2020;8:1071–83.
- [38] Zhang J, Chen X, Xia D, Huang G, Tang A, Jiang B, et al. Improving performance of friction stir welded AZ31/AM60 dissimilar joint by adjusting texture distribution and microstructure. *Mater Sci Eng, A* 2020;778:139088.
- [39] Li GH, Zhou L, Zhang HF, Guo GZ, Luo SF, Guo N. Evolution of grain structure, texture and mechanical properties of a Mg–Zn–Zr alloy in bobbin friction stir welding. *Mater Sci Eng, A* 2021;799:140267.
- [40] Steiner MA, Bhattacharyya JJ, Agnew SR. The origin and enhancement of {0001} <11-20>texture during heat treatment of rolled AZ31B magnesium alloys. *Acta Mater* 2015;95:443–55.
- [41] Beausir B, Biswas S, Kim DI, Tóth LS, Suwas S. Analysis of microstructure and texture evolution in pure magnesium during symmetric and asymmetric rolling. *Acta Mater* 2009;57:5061–77.
- [42] Nandan R, Roy GG, Lienert TJ, Debroy T. Three-dimensional heat and material flow during friction stir welding of mild steel. *Acta Mater* 2007;55:883–95.
- [43] Zhao J, Wu CS, Su H. Ultrasonic effect on thickness variations of intermetallic compound layers in friction stir welding of aluminium/magnesium alloys. *J Manuf Process* 2021;62:388–402.
- [44] Hu Y, Liu H, Fujii H, Ushioda K. Effect of ultrasound on microstructure evolution of friction stir welded aluminum alloys. *J Manuf Process* 2020;56:362–71.
- [45] Gao S, Wu CS, Padhy GK. Material flow, microstructure and mechanical properties of friction stir welded AA 2024-T3 enhanced by ultrasonic vibrations. *J Manuf Process* 2017;30:385–95.
- [46] Gao S, Wu CS, Padhy GK, Shi L. Evaluation of local strain distribution in ultrasonic enhanced Al 6061-T6 friction stir weld nugget by EBSD analysis. *Mater Des* 2016;99:135–44.
- [47] Fonda RW, Bingert JF. Texture variations in an aluminum friction stir weld. *Scripta Mater* 2007;57:1052–5.
- [48] Suhuddin UFHR, Mironov S, Sato YS, Kokawa H. Grain structure and texture evolution during friction stir welding of thin 6016 aluminum alloy sheets. *Mater Sci Eng, A* 2010;527:1962–9.
- [49] Siu KW, Ngan AHW, Jones IP. New insight on acoustoplasticity – ultrasonic irradiation enhances subgrain formation during deformation. *Int J Plast* 2011;27:788–800.
- [50] Liu Y, Suslov S, Han Q, Hua L, Xu C. Comparison between ultrasonic vibration-assisted upsetting and conventional upsetting. *Metall Mater Trans A* 2013;44:3232–44.
- [51] Du N, Qi Y, Krajewski PE, Bower AF. Aluminum $\Sigma 3$ grain boundary sliding enhanced by vacancy diffusion. *Acta Mater* 2010;58:4245–52.